UNIVERSITÀ DEGLI STUDI DI UDINE

DIPARTIMENTO POLITECNICO DI INGEGNERIA ED ARCHITETTURA
Corso di laurea magistrale in
Ingegneria per l'ambiente e l'energia, cl. LM-22

Tesi di laurea

Catalytic methane steam reforming in a micro-structured reactor for hydrogen production.

Relatori:
Prof. Alessandro Trovarelli
Prof. Jordi Llorca Piqué

Correlatrice:
Dott. Isabel Serrano Carreño

Laureando:
Gaetano Corsaro

ANNO ACCADEMICO 2017/2018

INDEX

ABSTRACT

In this project, a stainless steel micro-structured reactor built by a company for the hydrogen production by methane steam reforming is tested. A nickel based catalyst is prepared through the “incipient wetness technique” and deposited with different methods. The best result is achieved by depositing a pre-formed intermediate layer of alumina on the chromium oxide layer.

The reactor’s performance is compared with a cordierite monolithic reactor filled with the same catalyst to observe benefits and critical issue.

The results obtained show a production of hydrogen about 20% less than the cordierite reactor.

1. INTRODUCTION

1.1. Objective.

Hydrogen is one of the best energy vectors in terms of reduced emissions of pollutants and greenhouse gases. However, the implementation is still a challenge because of the technical and economic barrier to build a hydrogen energy infrastructure. For this reason, a distributed hydrogen infrastructure does not currently exist, although the technologies to produce, store and distribute hydrogen are matures and commercially available today.

A solution could be the production of hydrogen via small scale reforming, which is for sure less expensive than centralized production and subsequent distribution. Once the hydrogen demand increases, central hydrogen production would became cost competitive, considering also the opportunity of the carbon capture plants.

Fuel cells are an attractive option for reliable backup power, recognizing the vulnerabilities of grid dependency, as a fuel cell transforms hydrogen and oxygen (air) directly into electricity.

Many companies such as Bloom Energy or Doosan build equipments equipped with a reformer and a fuel cell in the same container, which can be used in stationary application to produce electricity and heat.

These companies usually install in their equipments SOFC or PEMFC. The solid oxide fuel cell has the advantage of the fuel flexibility, namely hydrocarbon fuels can be consumed, like natural gas, which is essentially constituted by methane.

This happens thanks to the high operating temperature around 650-1000 °C, that enables catalytic processes like the methane steam reforming. At these temperatures, the methane and the steam reacts catalytically producing hydrogen and carbon monoxide, which can be also converted into carbon dioxide by the water gas shift reaction (the methane steam reforming is discussed in more detail in paragraph 2.1). Another way to use methane as fuel can be the direct oxidation, but it is not feasible for the kinetic reasons and for the carbon deposition on the electrode.

Thus, it is easy to understand that the way to use the fuel affects both the performance and the layout of the entire plant.

Basically, there are three routes to use the hydrocarbon fuel in a SOFC: internal, external and partial pre-reforming.

In the internal reforming, the methane reacts with water steam directly in the electrode of the fuel cell. The heat needed to make the reaction takes place is directly provided by the operating fuel cell. However, only the methane can be used as fuel, because the higher hydrocarbons tend to lead carbon deposition on fuel cell anode.

The second method is the external reforming. All kind of hydrocarbon can be reformed and used as fuel, because the reforming takes place in a separated unit. The reaction occurs through HSR (heated steam reforming) or POX (partial oxidation). The second way is easier to design because it does not require a heater and a steam generator, even if it has a lower efficiency [1].

The third case is actually a combination of the first two, and it only can be used when the principal fuel is methane, for example natural gas or biogas. The fuel is processed in a pre-reformed where all the higher hydrocarbons are reformed or partially oxidised. Then, the rest of the gases finish the reforming process in the fuel cell stack.

The composition of the fuel gases influences the open circuit potential of the SOFCs as it is shown in Fig. 1 [2].

Fig. 1. Influence of Gas Composition of the Theoretical Open-Circuit Potential of SOFC at 1,000 °C [2].

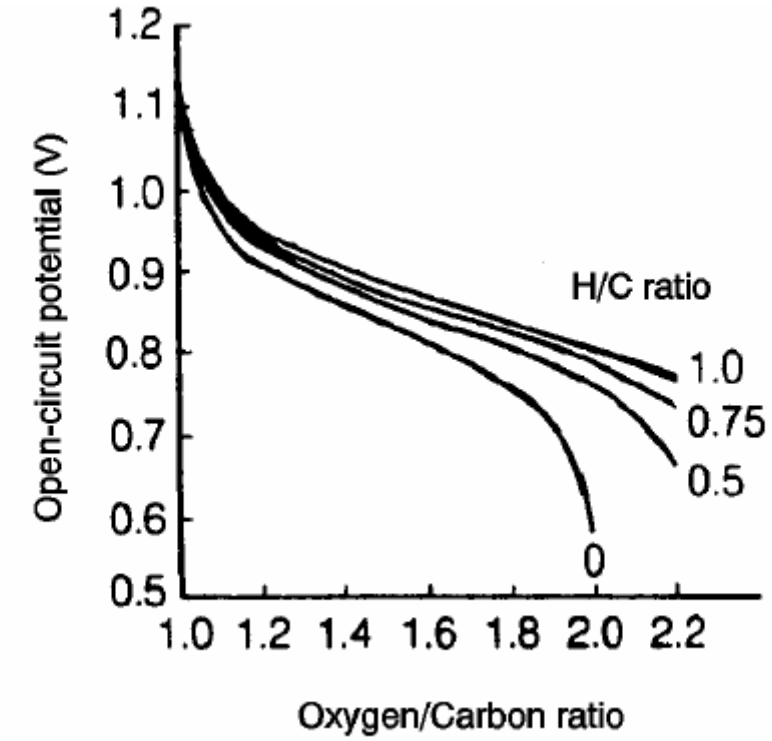

The oxygen/carbon (O/C) atom ratio and hydrogen/carbon (H/C) atom ratio define the fuel composition, and they are plotted as a function of the theoretical open circuit potential at 1000 °C. The Fig.1 shows that the theoretical potential decreases from about 1 V to about 0.6 V as the amount of O_2 increases and the fuel gas composition changes from CO to CO_2. The presence of hydrogen in the fuel increases the potential and the O/C ratio.

For this reason, it is better to use the largest amount of pure hydrogen, if it is convenient from an economic point of view.

Stationary fuel cells are becoming a serious alternative to Sterling engine, Organic Rankine cycle, and internal combustion engines for the generation of electrical power and the co-generation of heat as part of micro-CHP plants.

Asia-Pacific is currently the largest market for micro-CHP and it will probably continue to dominate this market. Japan is the market leader in fuel cell technology and it provides subsides for the development of it. In particular, this market is led by the residential sector [3].

In Europe, the leading country in micro-CHP area is Germany, and its experience serves the european demonstration program called “Ene.field”, which aims to install around 1000 fuel cell micro-CHP systems in 12Member States by 2020.

A typical plant scheme for external steam reforming is shown in Fig. 2.

Fig.2. Fuel cell plant’s scheme.

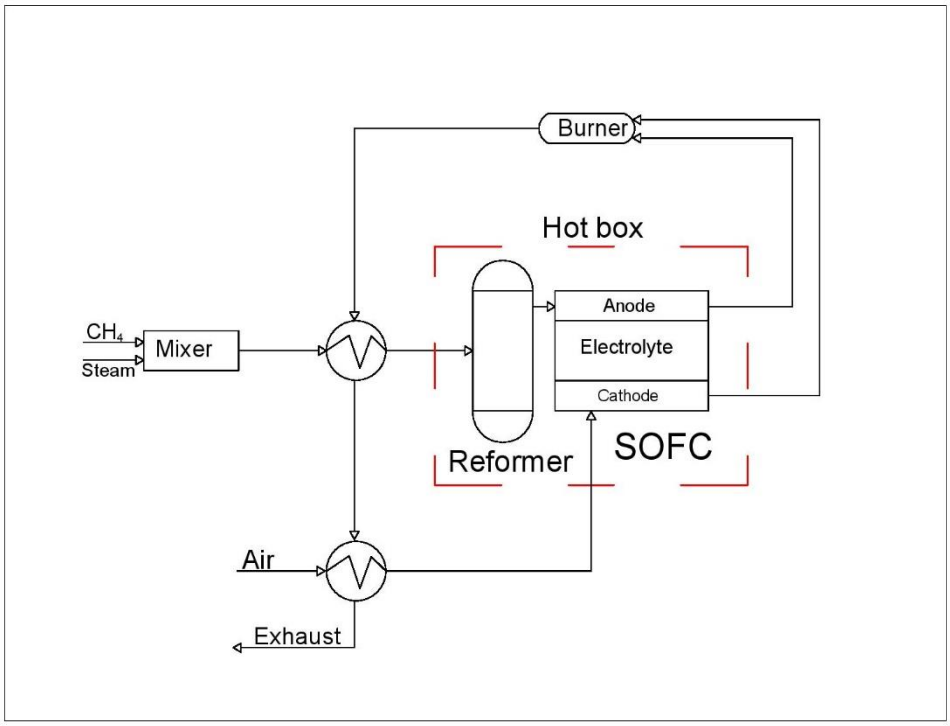

The steam and the methane are mixed, pre-heated and filled into the reformer. Then the gases enter into the fuel cell where they are oxidised. At the end, the exhaust gases are burned to complete the oxidation and the energy of the exhaust is recovered by the pre-heater.

These systems usually operates like a furnace, water heater, and electricity provider, and they can include a back–power system or other auxiliaries. The size is around 1-5 kW.

As has been said before, the implementation of SOFC in the residential sector has great advantages in environmental terms, because the NO_x production is completely avoided and the carbon dioxide production is reduced. K.U Birnbaum (et al.) [4] estimate a potential reduction of 1-4% of carbon dioxide in the residential sector in the OECD countries, evaluating different scenarios of fuel's cell diffusion by 2050.

In this project, the part concerning the methane steam reforming will be further investigated, in particular a company has requested to optimize the performance of a metal micro-structured reactor of its own production, that it will work as external reforming unit for a SOFC. Therefore, the main objectives are to find the right catalyst, the best way to deposit it, and finally test it under operating conditions.

1.2 Methane steam reforming

The methane steam reforming takes place by means of three reversible reactions.

$$CH_4 + H_2O \leftrightarrow CO + 3H_2 \qquad \Delta H°_{298} = +206\ \frac{kJ}{mol} \qquad (1)$$

$$CO + H_2O \leftrightarrow CO_2 + H_2 \qquad \Delta H°_{298} = -41\ \frac{kJ}{mol} \qquad (2)$$

$$CH_4 + 2H_2O \leftrightarrow CO_2 + 4H_2 \qquad \Delta H°_{298} = +165\ \frac{kJ}{mol} \qquad (3)$$

The (1) and (3) are strongly endothermic, while the (2) which is called water-gas shift reaction is moderately exothermic, so the entire process is endothermic and it is favoured for high temperature. The process takes also place with volume expansion, so a low pressure encourages the process.

In the Fig. 3 is shown the equilibrium gas composition at 1 bar as a function of temperature for methane steam reforming.

Fig. 3. Equilibrium gas composition for steam reforming at 1 bar with S/C=1[5].

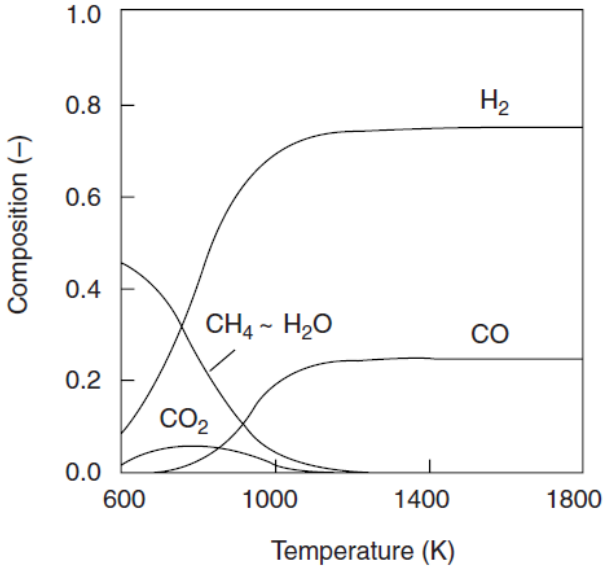

Due to the endothermic character, the production of hydrogen and carbon monoxide increases with temperature. Instead, the carbon dioxide reaches a maximum at low temperature due to the exothermic character of the water gas shift reaction, while for high temperature the endothermic reactions prevails, and it decreases because it is now a reagent.

The effect of the pressure is shown in Fig. 4.

Fig.4. Effect of pressure on equilibrium gas composition in steam reforming of methane, S/C=1 [5].

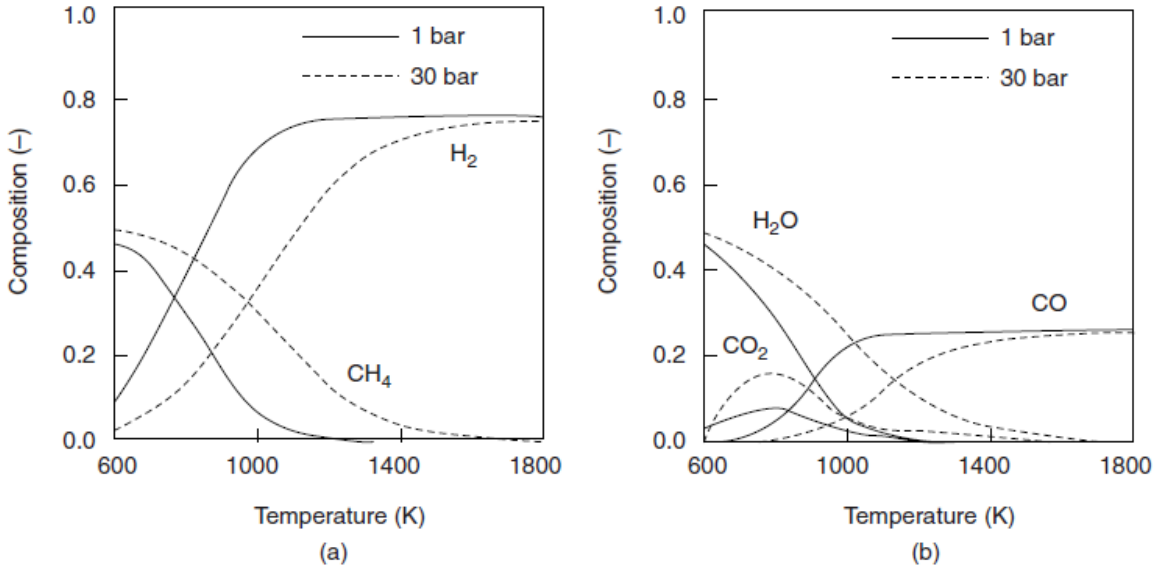

The complete conversion at 30 bar is only reached at a temperature over 1400 K, therefore the increase in pressure has an impeding effect.

As concern the kinetic, without going into details, Xu and Froment [6] developed a successful model, whose rate equations of the steam reforming reactions (1−3) are reported in Eq.(4).

$$r_i = \frac{k_i f_i(P_x,K_x)}{Z^2(P_x,C_x)} \; ; \qquad i = 1,2,3; x = CH_4, H_2O, CO_2, CO, H_2; \quad (4)$$

k_i are the rate coefficients of the reactions i, f_i are complex functions of partial pressure P_x , and equilibrium constants K_x. Z is a function of P_x and the adsorption constants C_x.

2. THE CATALYST'S CHOICE AND PREPARATION

2.1. Catalysts for steam reforming

To achieve a satisfactory production of hydrogen, a catalyst is essential to speed up the conversion rate of methane. The catalyst should be also stable and resistant to carbon formation under the working critical condition, besides being very active during the reaction.

Moreover, in order to obtain a faster hydrogen's production, it is necessary a high active surface area and in this case, the catalyst support plays the most important role.

In the steam reforming of methane, the most used catalyst in the chemistry industry is Ni due to its lower cost, although it is the less active among the metals that could be used (Ru, Rh, Pd, Ir, Pt) and the most susceptible to deactivation, carbon formation or oxidation [7].

In fact, the activity of the catalyst is not the only constraining factor, the reaction is controlled by the heating and mass transport phenomena [8].

Rostrup-Nielsen et al. ([7]and references therein) discovered that the dispersion or utilization of Ni tends to decrease with increasing nickel content. Consequently, the activity will not grow further.

The upgrade of Ni catalysts trough the addition of a small amount of noble metals such as Pt, Au, Rh has been well reviewed, and it has been shown many advantages in their application ([9]and references therein).

The catalyst must be fixed on a support to gain a more stable and higher active surface area. However, this is not the only role of the support; it works synergistically with the metal particles effecting the reactivity and the resistance to coke formation and sintering.

Furthermore, the final metal particle distribution is determined by the configuration and phase transition of the support.

Several supports have been studied and developed for methane steam reforming, such as $\alpha \; and \; \gamma - Al_2O_3$, $MgO, MgAl_2O_4, ZrO_2, SiO_2, TiO_2$, and all of them have a good porosity resulting in a high specific area. Nevertheless, the chemical properties of the support strongly

influence the catalyst's stability and chemical reaction. For instance, acidity of the support promotes the decomposition of methane, but on the other hand, it produces more carbon, facilitating polymerization and cracking [10]. Basic supports, like MgO, promote the activation of the steam (formation of OH and H) instead, reducing the coke formation [11].

Zang *et al* , studied the dry methane reforming on Ni/La_2O_3 [12], showing that, this catalyst is very stable, in contrast to traditional ones which show continuous deactivation with time on stream. The reason lies in the formation of $La_2O_2CO_3$, which is formed by reaction between La_2O_3 and CO_2.

The carbon formation is a challenge in the steam reforming processes. The probability of carbon formation is dependent on the S/C ratio. It increases with the temperature (above 450°C) [7]. The main reactions that bring carbon formation are [13]:

$$CH_4 \leftrightarrow C + 2H_2 \quad (5)$$

$$2CO \leftrightarrow C + CO_2 \text{ (Boudouard)} \quad (6)$$

$$CO + H_2 \leftrightarrow C + H_2O \quad (7)$$

This is explained by the hydrocarbon dissociation that brings to an allotropic form particularly reactive (C_α). Due to high temperature, part of C_α undergoes a transformation into the less reactive form C_β, for the polymerization and rearrangement of C_α.

Three types of carbon formation occur: graphitic carbon, polymeric carbon and whisker.

The graphitic steams from the thermal cracking of hydrocarbons, and it forms a carbon layer that prevents gas from reaching active sites.

The polymeric carbon is generated from the olefin polymerization in the pore structure. Here, the stress produced by the carbon can break the pellets, increasing the pressure drop.

The whisker is formed from dissociation of CO, CH_4 and higher hydrocarbons on the top of the metal particles, especially on the Ni. A continued growth can lead to the disintegration of the catalyst matrix due to the strong strength and an increase in the load losses of the reactor.

The boundary conditions for the formation of carbon are also a function of the crystalline grain of the nickel particle. In fact, the occurrence of whiskers will be at a higher temperature with a smaller size of particles [14].

Regarding the methane steam reforming, it is been shown that the importance of the carbon formation and the catalyst's stability at high temperature through different studies, therefore, many authors are still focusing on the Lanthanum effect on the Alumina support for hydrocarbon reforming [15]. In particular, the works on the dry steam reforming (with CO_2 instead of water) are interesting due to the critical working condition, such as high temperature and high carbon deposition.

R. Martinez et al. [16] showed the benefits of adding Lanthanum oxide to a Ni-Al catalyst, such as the stronger resistance to carbon formation and the higher stability, maintaining high activity over long reaction time. These positive effects are attributable to the better metal distribution, where there is a narrower NiO particle size distribution in samples containing lanthanum.

The advantages of adding La on alumina support can be observed also for FeCrAl alloy [17]. Especially better results in washcoating of FrCrAl alloy are due to:

- High surface area at temperature up to 1200 °C because La stabilizes the metastable phases of La_2O_3 trough the prevention of α-transformation.
- The La_2O_3 has a zeta potential able to control the high pH region, hence the alkaline solution is applicable to the alloy substrates.
- The layer doesn't have significant breakages up to 1200 °C.
- The Lanthanum modification leads to a better composite structure of the porous coat and to a strong bond with alloy substrate.

2.2 Catalyst preparation

In accordance with the discussion about the $Ni - La - Al_2O_3$ catalysts, it is clear that this kind of catalyst could be the best choice for our purpose, achieving a good compromise between cost and performance.

The kinds and the amount of substance used to synthetize the catalyst are detailed below:

- $Al(OH)_3$ (90% Panreac) 69 wt.%

- $La(NO_3)_3 \cdot 6H_2O$ (99% Panreac) 3,7 wt.%
- $Ni(CH_3COO)_2 \cdot 4H_2O$ 27,3 wt.%

Besides these, NH_3 (28%) and distilled water are also used.

The catalyst's precursor salts support are added and dissolved with 150 ml of distilled water in a Erlenmeyer Flask. When the salts are dissolved, the co-precipitation can start, in the meantime adding gradually 20 ml of NH_3 until the pH reaches a value of 9-10, while the mixture is agitated. Afterwards it is aged without temperature all night long.

Next, the precipitate is filtered and washed ten times with the same amount of distilled water that was used to prepare the mixture.

The precipitate is dried at 70-80 °C during 3 hours, and after that, increasing the temperature up to 120°C until it is completely dry. Then, it must be calcined at 600 °C for 5 hours using a ramp programme of 5 °C/min.

Then, a solution of Ni in water is added in the powder obtained, following the incipient wetness method.

Fig. 5. Same steps of incipient wetness method.

In this way, the active phase is transported into the pores by the capillary force and not by the diffusion process that occurs when the solution is in excess. Thus, the powder is impregnated with the dissolution, and on each step it is dried at 80 °C.

Finally, the product is kept in the oven at 120 degrees all night long, and then it is calcined at 400 °C for 5 hours using a 2 °C/min ramp.

Fig.6. Catalyst after calcination at 400°C.

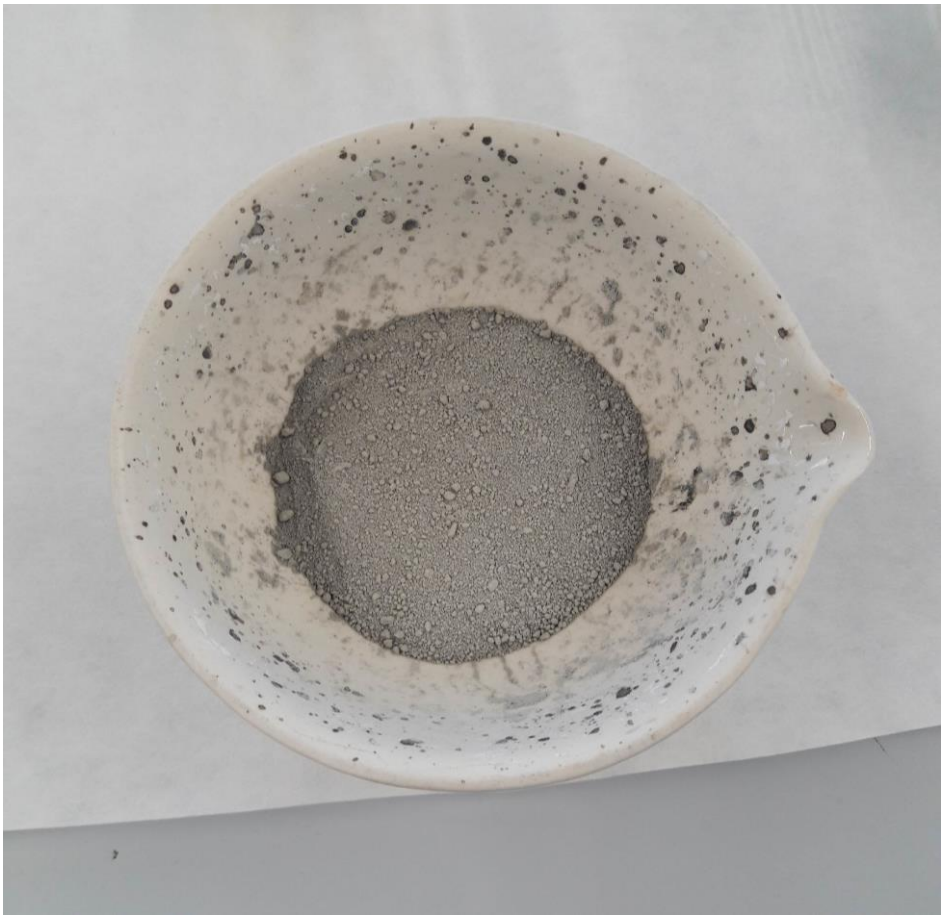

3. CORDIERITE MONOLITHIC REACTORS ASSEMBLY.

3.1 Monolithic reactors

Monolithic supports are single structures made up of many channels or cells interconnected, and it involves a high surface area, but a low pressure drop due to the little flow resistance.

The most common materials used for the preparation of monoliths are ceramics and metals, and rarely plastics [18]. The market of extruded monolith substrates is constantly growing since in mid-1970s, when the catalytic converter was installed in new vehicles in USA [19]. The material was $2MgO\ 2Al_2O_3\ 5SiO$, a ceramic called cordierite. The choice of cordierite is justified by some of its properties that make it suitable for this type of application. In particular, cordierite has a low thermal expansion coefficient, which involves a high thermal shock resistance, in addition to a sufficient strength. Moreover, it is very suitable for washcoating due to the high porosity and the good pore size distribution[20].

Due to complexity of fabrication technology, the metallic monoliths were marketed in the 1990s and they have a narrower market. The advantages of these types of monoliths are the low pressure drop and the high cells density. In addition, the metal has a high heat transfer coefficient, so they are suitable for applications that require a supply of a high amount heat, even if we must consider the greater expansion coefficient, which involves advanced bonding techniques to produce an adherent washcoat. Another issue that warrants attention is the corrosion at high temperature, and in fact special alloys are used such as FeCralloy.

3.2 Design of cordierite reactor

A cordierite monolithic reactor was prepared in order to compare its catalyst performance against the metal micro-structured rector.

As it is mentioned earlier, the cordierite reactors have been widely studied and it is used in several applications for the good adherence of the catalyst. Therefore, once the ceramic reactor was built,

the same catalyst was introduced and tested under the same conditions of the other reactor. The reactor was modelled with a hacksaw from a larger cordierite honeycomb block.

The desired dimensions for the reactor are shown in the Fig. 7.

Fig.7. Cordierite reactor size.

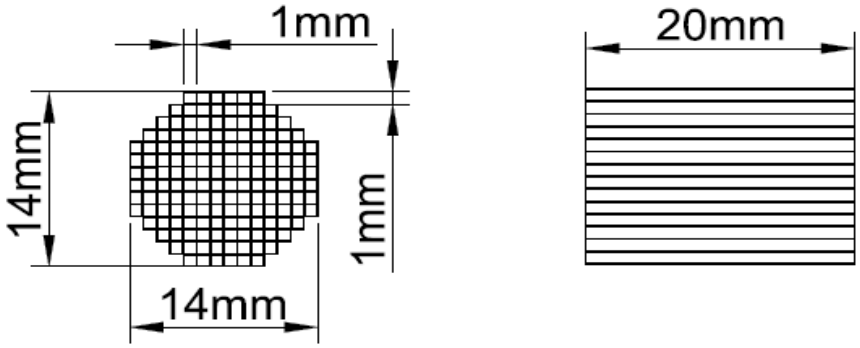

Fig.8. Cordierite reactor 3D model.

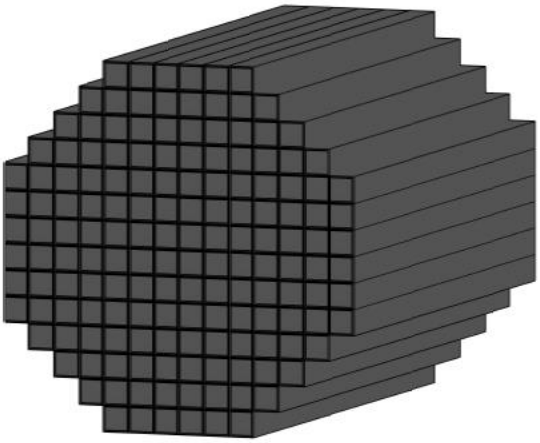

At the end, four monoliths have been built, and respectively named A1, A2, A3 and A4 (Fig.9).

Fig.9. Cordierite monolithic reactors, samples A1,A2,A3 and A4.

3.3 Catalyst deposition

A nude monolithic reactor can be coated with a layer of catalyst support to have a better adherence between the reactor surface and active metal. Preparing and deposing a “coat” for the catalyst is a procedure called wash coating or dip-coating, and basically there are several ways to perform it. Coating using colloidal solutions, sol-gel coating, slurry coating are the most common, but techniques such as chemical vapour deposition, sputtering and polymerization coating for carbon support are also possible [21]. In the first one, the monolith is dipped into a colloidal solution of the washcoat material (alumina, silica, etc). After the extra fluid is thrown out, the monolith is dried rotating it horizontally around its axes to distribute the liquid inside evenly, and at the end calcined at around 400-500 °C to fix the catalyst layer.

The sol-gel procedure differs from the previous for the physical characteristics of the sol. In fact, the coat is dissolved in the liquid to form a gel. In this way is easier to reach all pores. An example

of an alumina sol-gel coat is reported by [22]. A commercial colloidal pseudo-boehmite (γ-AlOOH) powder was calcined at a range of 500-700 °C to convert it to γ-alumina phase. Then, HNO_3 was used to adjust the pH at 4 and two different, highly viscous PVA-based binders were added to increase the viscosity. At the end, the cordierite specimens were immersed in the sols for 1 min and dried with the techniques shown before.

In slurry coating, at the beginning of the process the material must be wet-milled. In this way the reactants flowing through the channels have a shorter diffusion distance to the active catalyst species and the monolith macropore volume does not limit the maximum loading of the coat. To achieve this, slurry of particles must have a comparable size as the larger macropores of the support (few micrometers).

In this work, the active metal is previously placed on the support.

A sol-get coat was prepared adding 9 wt% of Polyvinyl alcohol (PVA), 1 wt% of acetic acid CH_3COOH and water in two bakers, and then continuously shaken at 75 °C until the PVA becomes a gel with a suited viscosity. Now the 4 g of catalyst is added, with a continuous mixing, until uniform distribution is obtained.

The cordierite monoliths were immersed inside the bakers (2 monoliths each baker) until air bubbles came out. After that, the coated samples were dried at 100 °C for 1 h in the oven, rotating it horizontally around its axes to avoid a bad catalyst distribution.

Fig.10. Rotating system for monoliths drying.

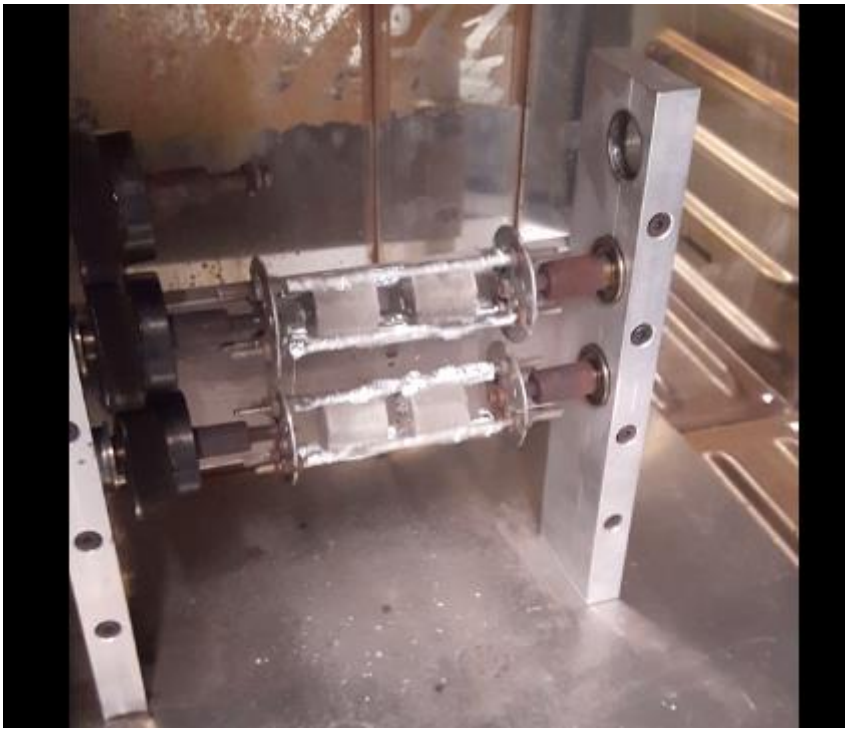

At the end, the monoliths were calcined at 400 °C for 1h with a 10 $\frac{^{\circ}C}{min}$ ramp. The result after the calcination are shown in Fig.11. where it is easy to see the PVA ejected from the channels.

Fig.11. Monoliths after calcination at 400 °C.

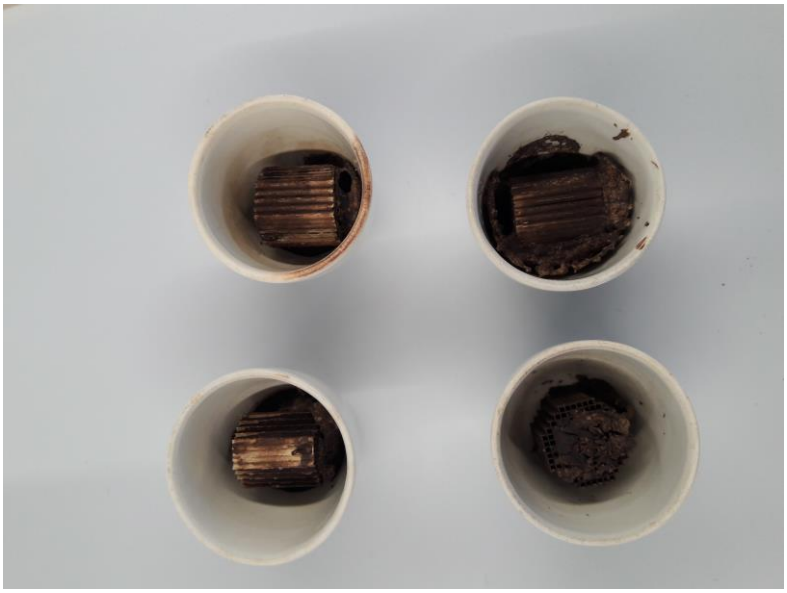

The dip coating process was repeated seven times to reach around 500 g of catalyst inside each monolith. The Table 1 shows the weight increase for each monolith.

Tab.1. Dip-coating process, catalyst weight increase.

	T0	**T1**	**T2**	**T3**	**T4**	**T5**	**T6**	**T7**
A1 [g]	*2,410*	*2,598*	*2,634*	*2,750*	*2,805*	*2,917*	*2,981*	-
A2 [g]	*2,238*	*2,393*	*2,438*	*2,526*	*2,594*	*2,684*	*2,741*	-
A3 [g]	*2,488*	*2,694*	*2,711*	*2,777*	*2,857*	*2,894*	*2,988*	-
A4 [g]	*2,441*	*2,608*	*2,637*	*2,700*	*2,778*	*2,816*	*2,906*	*3,003*

Instead, the final catalyst weight for each sample is summarized in Tab.2.

Tab.2. Final catalyst weight.

A1	571 mg
A2	503 mg
A3	500 mg
A4	562 mg

4. CATALYST DEPOSITION ON METAL MICRO-STRUCTURED REACTOR

4.1 Reactor design

The company built the micro-structured reactor from the sintering of powders of a stainless steel, which composition is reported on the paragraph 4.2 Table.3. The structure is quite simple: seven plates are scratched to form seven micro-channels, and then they are separately inserted into the cylindrical body. The dimensions of the reactor are reported in Fig.12.

Fig.12. reactor's dimensions (mm).

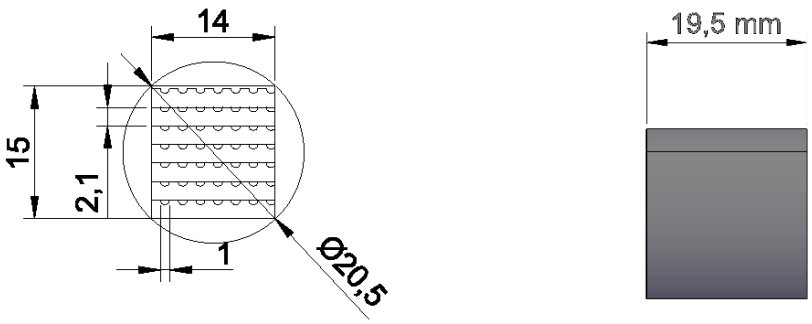

And the Fig.13 shows how it looks like.

Fig.13. Micro-structured reactor.

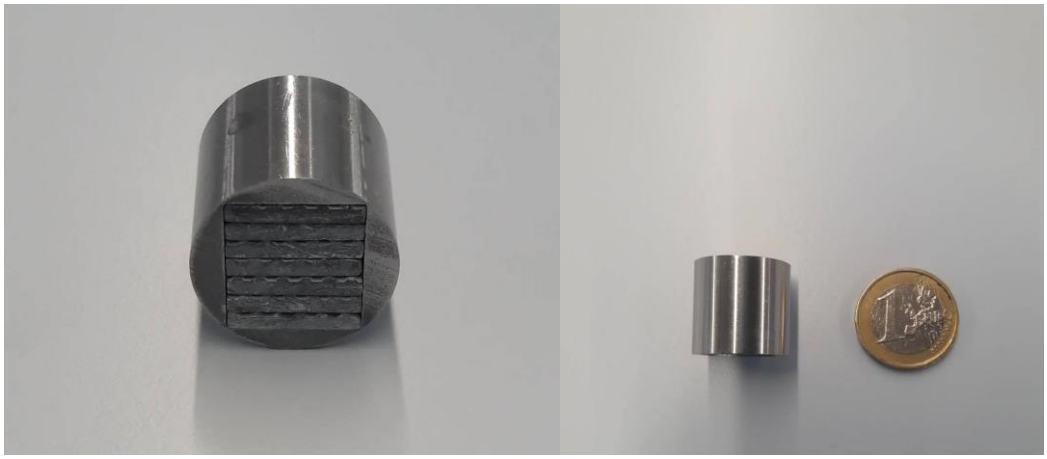

It should be noted that the plates are not all about the same height, so the block of the seven plates must be carefully chosen in order that all the plates can enter avoiding an extra space that allows unwanted movements.

4.2 Reactor's metallic Alloy

The company provided the plates metal composition. They are composed of a FeCralloy with a little percentage of Mo and Mn. The exact percentages can be found in Table 3.

Tab.3. Alloy composition.

Fe	76,0%
Cr	22,4%
Mo	0,64%
Mn	1,09%

The main issue for the catalyst deposition is the adherence with the metal plate. The most common path in order to overcome this problem is to form an oxide layer, which can be typically formed chemically, thermally or anodically. The way chosen in this project is the thermal oxidation, as it is the easiest and cheapest way.

It is crucial in this respect to look at the Fe-Cr phase diagram Fig.14., since the chromium is the most important element of our alloy and it is the one that defines the stainless steel characteristics when the temperature changes.

Fig.14. Fe-Cr phase diagram [23].

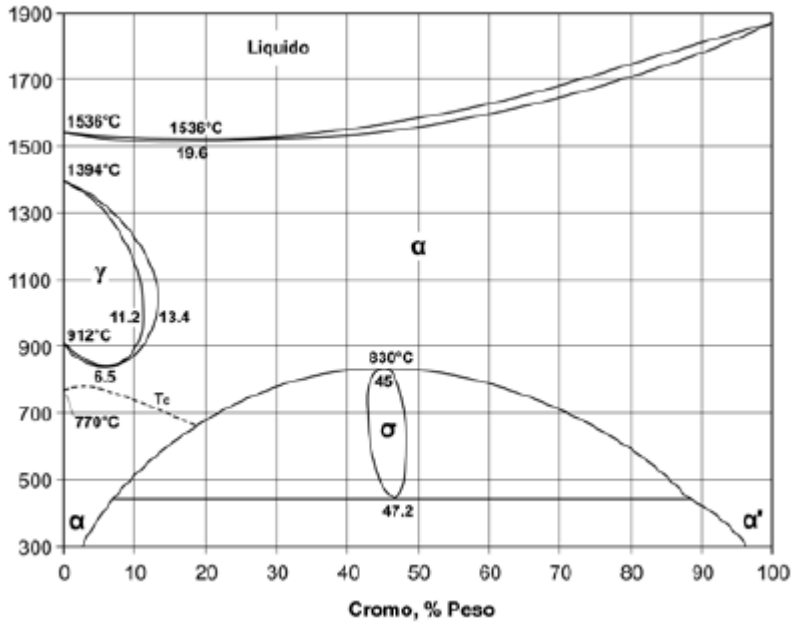

As chromium is a ferritizing element, namely it promotes the enlargement of the existence field of the α phase, the Fe-Cr diagram shows a closed γ phase, which means that if the chrome content exceeds 13,4%, the alloy will have an α reticle, stable starting from the solidification temperature of the alloy up to room temperature.

Thus, as it is shown in the diagram, it is possible to form an oxide layer heating the metal plates up to 1500 °C without changing significantly the metal properties.

4.3 Thermal pre-treatment.

Unlike the ceramic reactors, the metal reactors are not so easy to coat due to the poor roughness and chemical compatibility. In fact, in this case, a previous step is required, which involves the alteration of the metal surface to increase the adherence with the coat. The pre-treatment will depend on the composition of the metal alloy and it is usually headed to the

formation of an oxide layer chemically compatible with the catalyst and having a roughness which promotes the mechanical anchoring of the coat.

O.H. Laguna *et al* [24] have summed up all the metallic substrate pre-treatment methods. Based on the alloy composition, as it was shown before, the methodology changes. Thus, with an aluminium alloy anodic oxidation is preferred to make a thin alumina layer on the metal surface, and the characteristics (thickness, density and pore structure) of this last depend on the anodizing condition.

However, for the alloys that do not contain aluminium, it is usually used the thermal pre-treatment, because with a range temperature of 800 – 1000°C is possible to form a layer of oxides whose composition depend on the alloy, the temperature and the processing time. It enables to increase more or less the roughness and therefore the anchorage, which is also improved by a more similar thermal expansion coefficient. In this way, it is possible to lose less catalyst working at high temperature.

Y.Diaz *et al.* [25] for example, worked with an AISI 304 alloy, which is mainly composed of Fe, Cr and Ni, using a temperature of 950°C for 3 hours and achieved good results.

Against this background, considering also the high level of chrome and molybdenum in this alloy, the metal plates of the reactor have been placed inside the muffle furnace for 4 hours at 1000°C.

Before this treatment, the plates have been carefully cleaned with acetone to remove all the impurities deposited on the surface during the cutting procedure.

The result and the look of the metals before and after the calcination is shown in the Fig.15.

Fig.15. Metal plate before and after calcination at 1000°C for 4 hours.

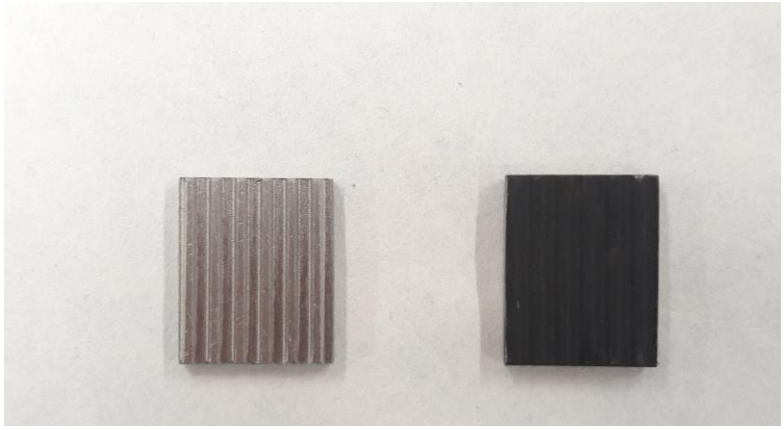

After the treatment, the plate is homogeneously black. A scanning electron microscope (SEM) allows to check in greater details the difference of the surface before and after the treatment, in particular the oxide layer.

Fig. 16 shows the SEM image of the metal plate surface without any treatment for different magnifications.

Fig.16. Scanning electron microscopy images of the surface morphology of the plates for different magnifications, without treatments.

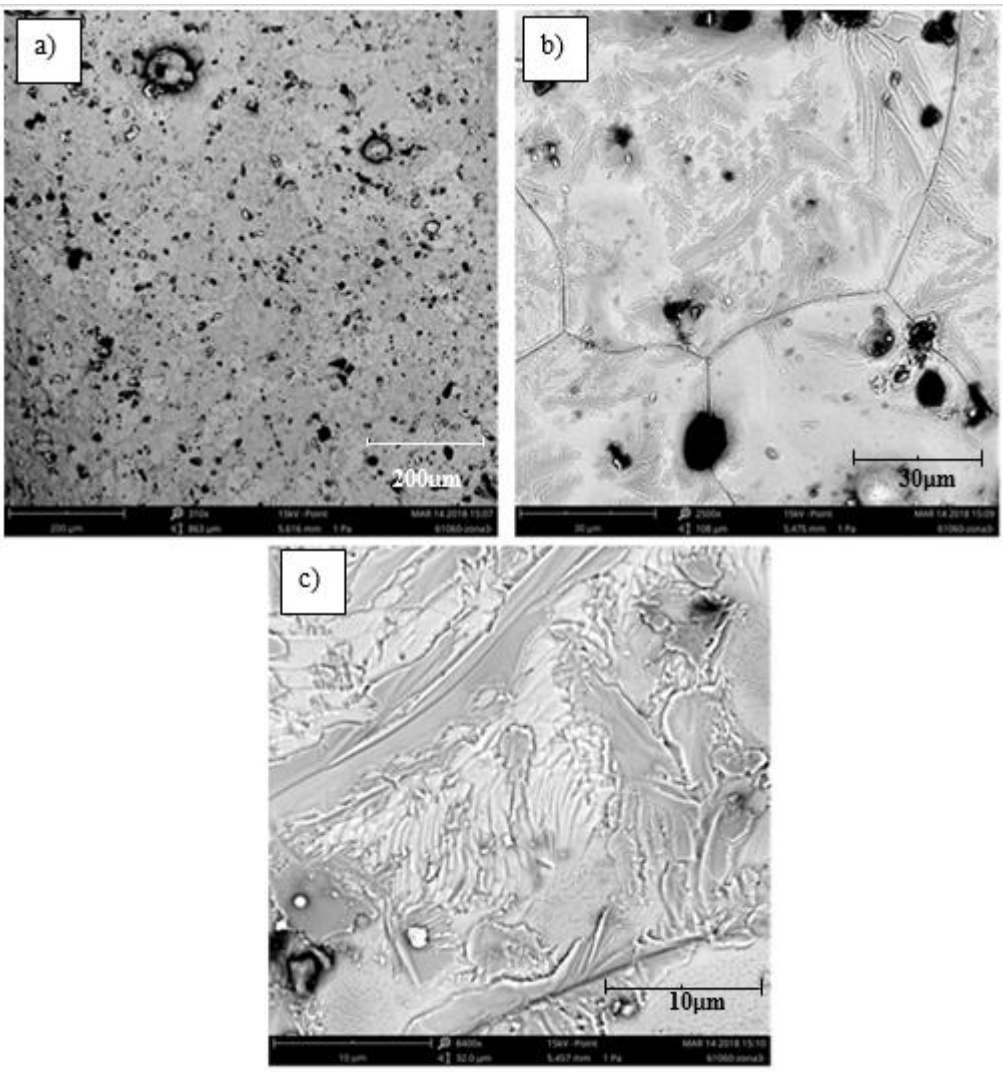

In the first magnification Fig. (a) it is already possible to see the orientation of crystalline grains, impurities due to the metal cutting (black points), and mostly important, the low roughness of the surface, which is even more clear to notice in the magnification (c). In fact, the grain has only few thin ripples that do not probably allow a strong anchorage.

Thanks to SEM-EDX (Energy-dispersive X-ray spectroscopy) it was also possible to provide a qualitative analysis of the surface composition of the metal plate. The analysis was performed on 3 random points in order to check any punctual differences. In the Fig.17 the position of the three points is given, and in the Figs.18,19 and 20 the corresponding EDX spectra with the weight percentage composition and the atomic concentration are shown.

Fig.17. Placement of analyses points.

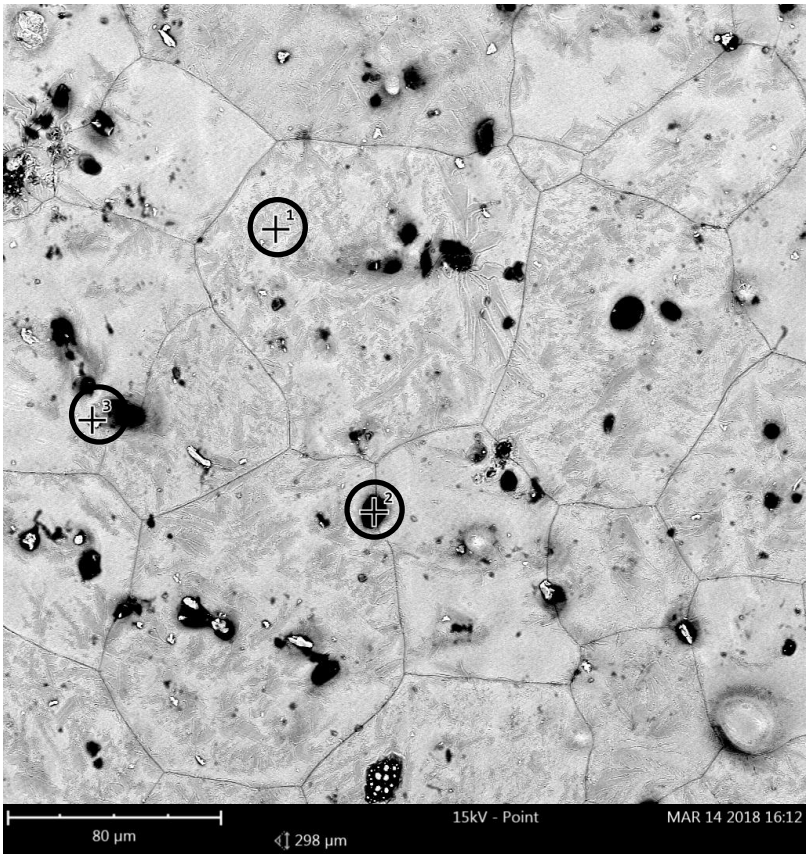

Fig.18. Spectrum and atomic-weight concentration point 1.

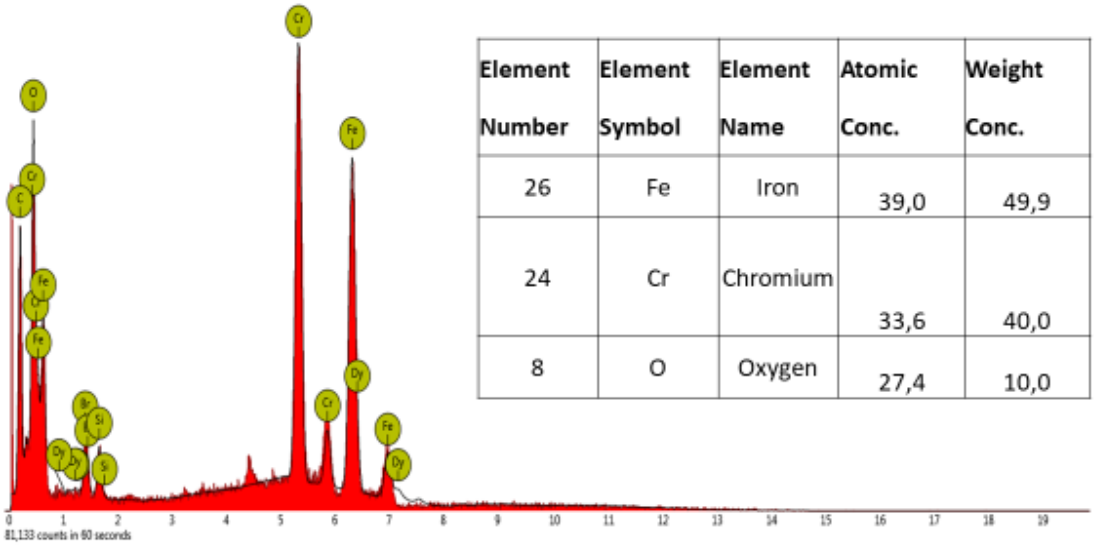

Element Number	Element Symbol	Element Name	Atomic Conc.	Weight Conc.
26	Fe	Iron	39,0	49,9
24	Cr	Chromium	33,6	40,0
8	O	Oxygen	27,4	10,0

Fig.19. Spectrum and atomic-weight concentration point 2.

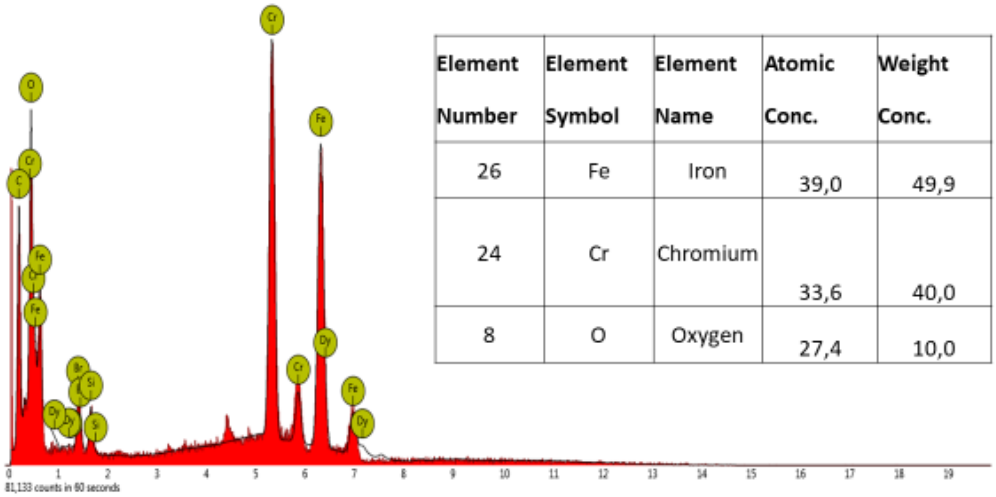

Element Number	Element Symbol	Element Name	Atomic Conc.	Weight Conc.
26	Fe	Iron	39,0	49,9
24	Cr	Chromium	33,6	40,0
8	O	Oxygen	27,4	10,0

Fig.20. Spectrum and atomic-weight concentration point 3.

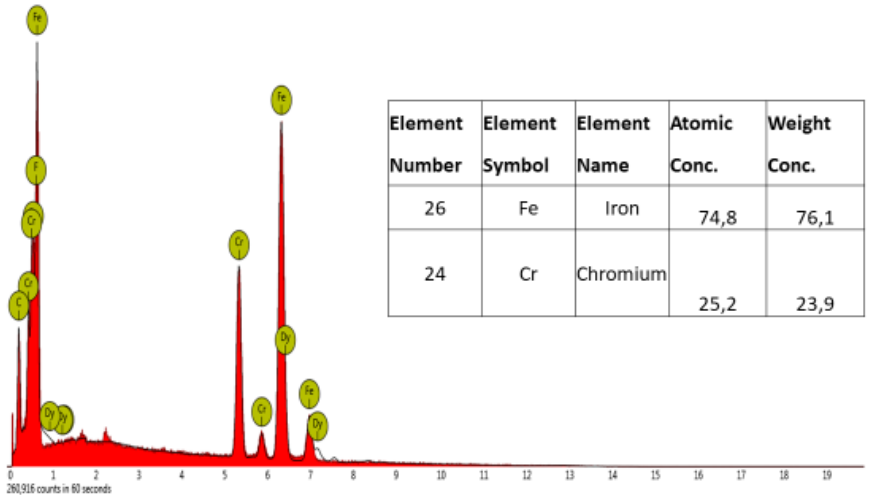

Element Number	Element Symbol	Element Name	Atomic Conc.	Weight Conc.
26	Fe	Iron	74,8	76,1
24	Cr	Chromium	25,2	23,9

The SEM-EDX study has been performed also for the plate subjected to the thermal treatment to confirm if the oxide layer has effectively raised the surface's roughness. This was confirmed by the pictures shown in the Fig.21.

Fig.21. Scanning electron microscopy images of the oxide morphology for different magnifications, for the plate with thermal treatment, 1000°C for 3 hours .

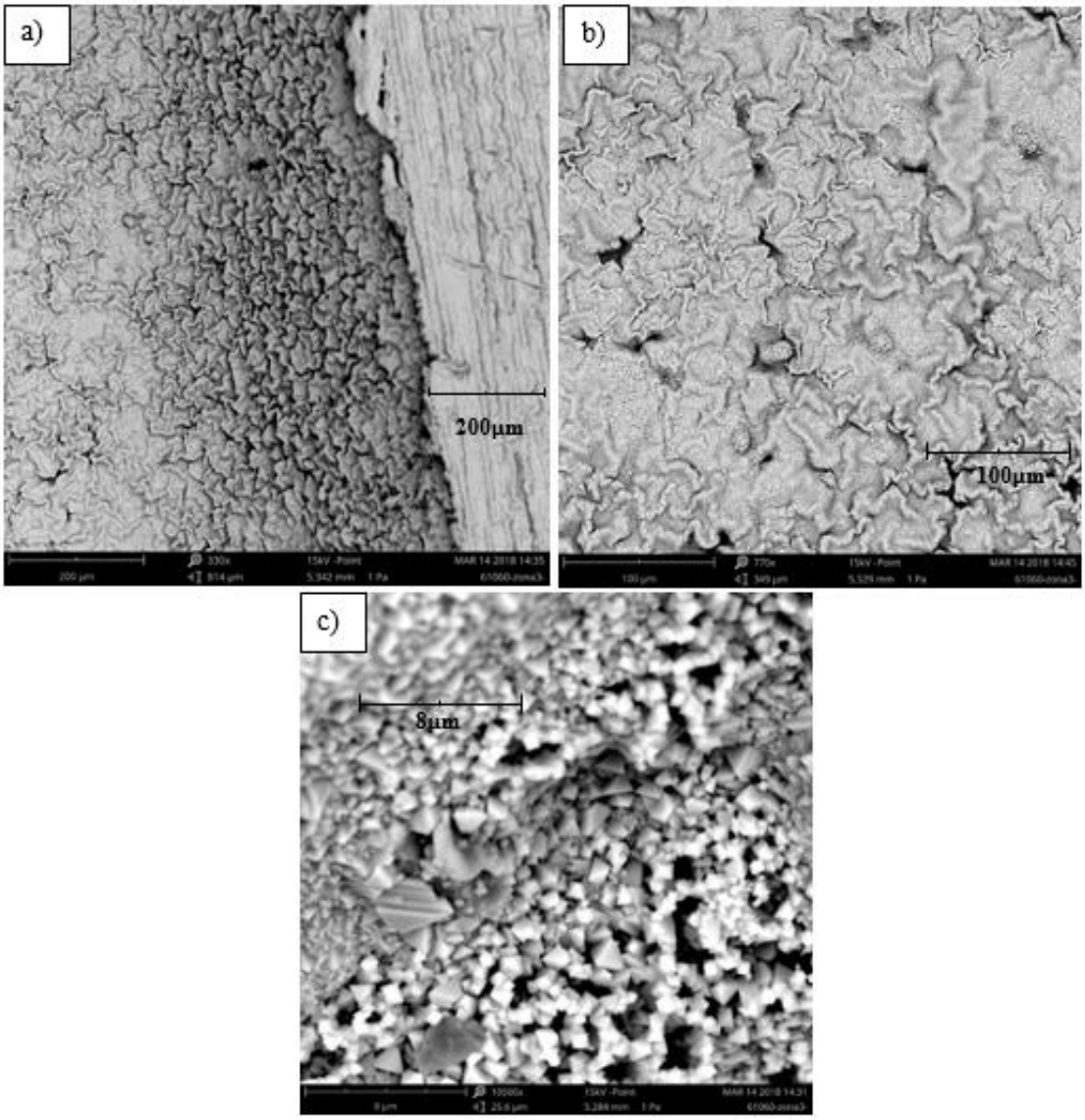

As the pictures shown, the change of the plate's colour after the treatment is due to the formation of a rugged layer on the surface. At low magnification the oxide layer is uniform, but with many grooves which could allow a better interaction with the catalyst eventually deposited. Increasing the magnification, also, the uniform slabs present a jagged and angular surface, consequentially, it is not wrong to think that a better anchorage is achievable.

In the same manner of the previous sample without thermal-treatment, the Energy-dispersive X-ray spectroscopy has been carried out on the plate thermally treated to give a qualitative analysis of the oxide layer. The chosen random points are reported in Fig.22. and the spectra of the point are respectively shown in Figs. 23, 24 and 25.

Fig.22. Placement of analyses points.

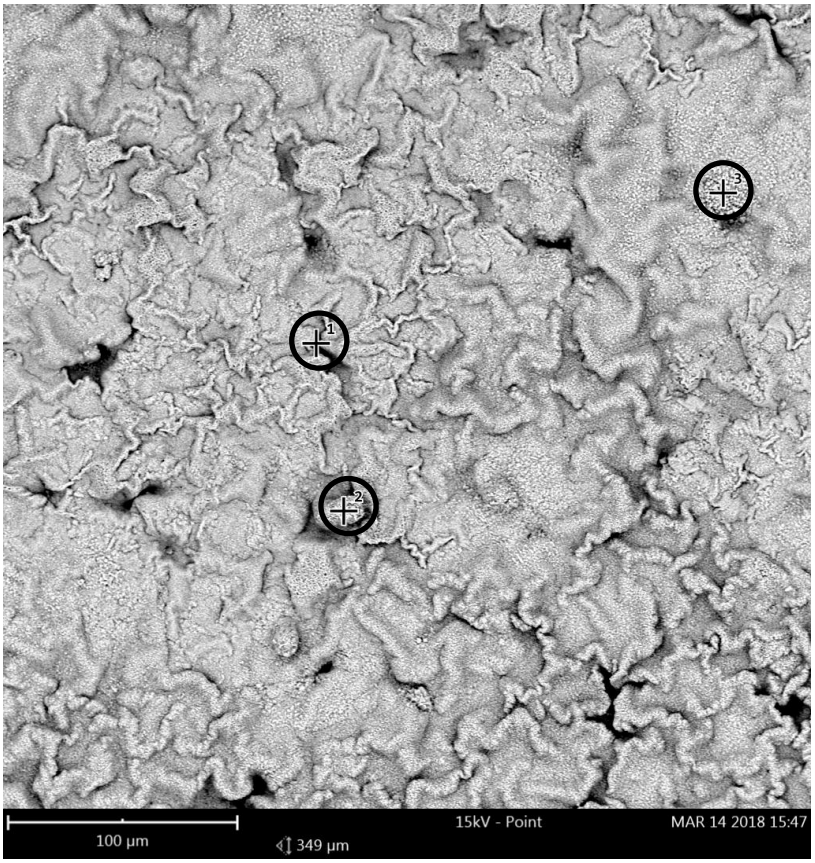

Fig.23. Spectrum and atomic-weight concentration, point 1, sample with thermal treatment.

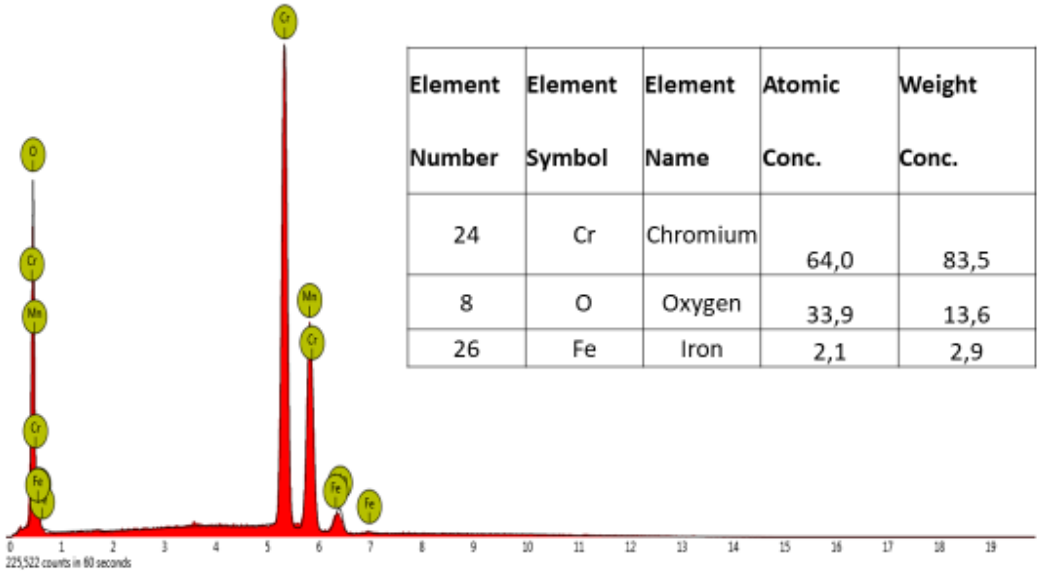

Element Number	Element Symbol	Element Name	Atomic Conc.	Weight Conc.
24	Cr	Chromium	64,0	83,5
8	O	Oxygen	33,9	13,6
26	Fe	Iron	2,1	2,9

Fig.24. Spectrum and atomic-weight concentration, point 2, sample with thermal treatment.

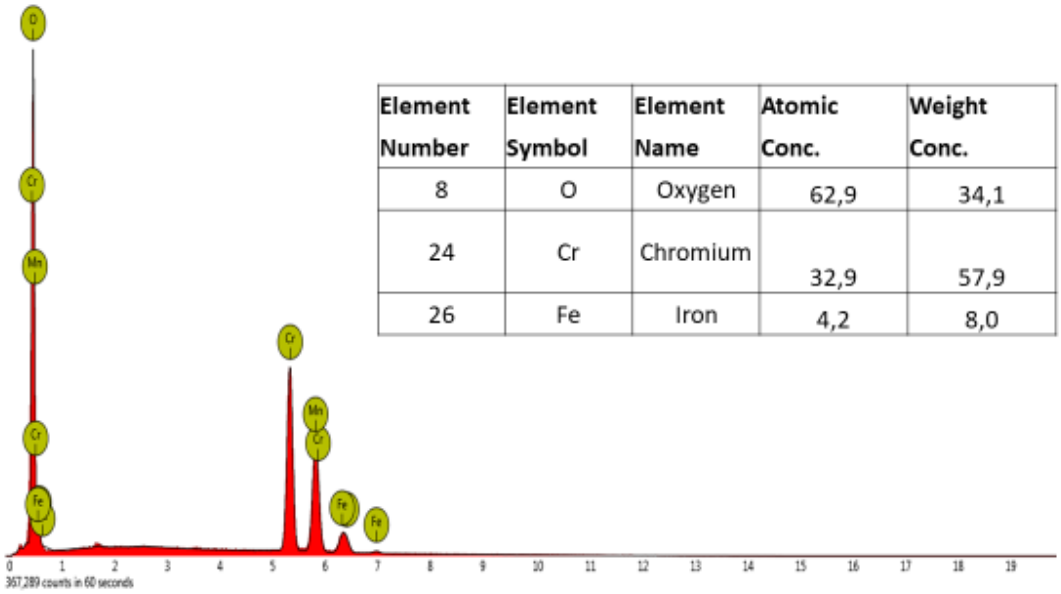

Element Number	Element Symbol	Element Name	Atomic Conc.	Weight Conc.
8	O	Oxygen	62,9	34,1
24	Cr	Chromium	32,9	57,9
26	Fe	Iron	4,2	8,0

Fig.25. Spectrum and atomic-weight concentration, point 3, sample with thermal treatment.

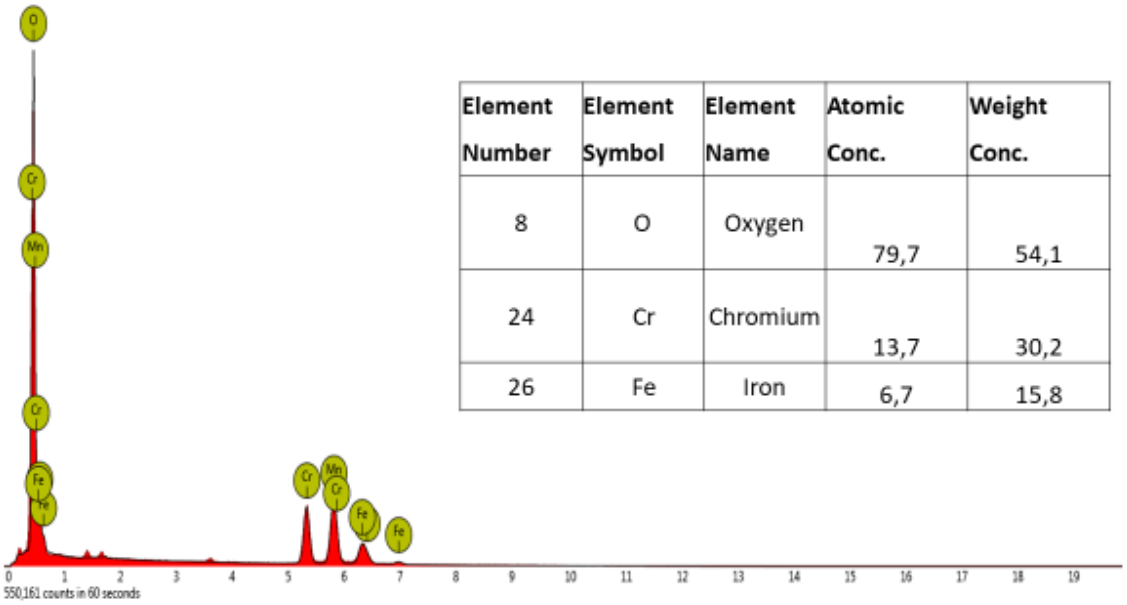

Element Number	Element Symbol	Element Name	Atomic Conc.	Weight Conc.
8	O	Oxygen	79,7	54,1
24	Cr	Chromium	13,7	30,2
26	Fe	Iron	6,7	15,8

As expected, the squared grains seen in Fig.21 are oxides, mainly composed by chromium, followed by iron.

4.4 Catalyst deposition.

The catalyst selected for the micro-structured reactor is the same of the cordierite monolith. As the cordierite reactor, several methods are available to deposit the catalyst preserving its properties as the crystalline phases, textural properties, and dispersion of the active phase.

The coating methods for a metal surface are basically divided into two categories: liquid-phase and vapour-phase methods, depending on the physical state of the coating medium[24].

Among the methods in liquid phase there are electrophoretic and electrochemical deposition, spray coating, in situ growth and wash coating, for the vapour-phase, chemical and physical vapour deposition are the most important.

For its simplicity and versatility, the dip-coating method seemed the best for this kind of application. However, due to the specificity of the reactor, it was necessary to find the best configuration by testing various options.

Initially, the tests were carried out on plates having a smaller area (14x14,9 mm^2) and they have been called sample P1, P2 and P5.

The oxide layer has been formed only on the sample P1 and P2, but not in the sample P5, to see if it is truly effective and thus necessary to increase the adherence.

Furthermore, the composition of the slurry is different for the various samples. On the sample P1 and P5, 5 mg of catalyst has been mixed in a solution of 5 ml of water, whereas Polyvinyl alcohol has been used as binder. The slurry composition and preparation is the same as the one used for the cordierite monolith and reported on the paragraph 3.3.

Table 4 compiles an overview of the sample specifications.

Tab.4. Samples P1, P2, P5 features.

Sample	Thermal treatment	Slurry composition
P1	Yes	5 ml of H_2O and 5 mg of catalyst
P2	Yes	1,25 g of PVA, 25 ml of H_2O, 475 µl of CH_3COOH and 1 g of catalyst
P5	No	5 ml of H_2O and 5 mg of catalyst

Once prepared the slurry, the deposition has not been carried out dipping the plate, but filling the plate's channels with the slurry using a syringe with a 12,5 mm needle.

After this stage, all the plates have been dried in the oven at 100 °C for 30 minutes and then calcined at 400 °C for 2 hours with a ramp of $\frac{10\,^{\circ}C}{min}$. These steps have been repeated several times to maximise the ratio catalyst weight on plate's area $\frac{mg}{cm^2}$, even if it was observed in a later stage, that it is not possible to fill all the plates in the reactor adding a high amount of catalyst on the plate. However, the correlation of this parameter with the adherence (measured with the percentage of weight lost in an ultrasound test) is still important to consider. In Table 5 the weight gain is shown.

Tab.5. Sample P1, P2 and P5 weight gain.

	Initial weight	**T1**	**T2**	**T3**	**T4**	$\boldsymbol{\frac{mg}{cm^2}}$
P1	2,059 g	2,065 g	2,070 g	2,080 g	2,102 g	21,3
P2	1,910 g	1,919 g	1,917 g	1,917 g	1,921 g	5,5
P5	2,652 g	2,665 g	2,674 g	2,684 g	2,701 g	24,4

It is interesting to underscore that the sample P2, the one where the catalyst has been deposited with the addition of PVA, does not substantially increase the weight after the first deposition and this is due to the non-uniform catalyst coat formed, which is shown in Fig.25 and in the SEM picture.

SEM-EDX has been used also to check the catalyst composition and its uniformity on the plate's surface. The samples P1 and P2 have been analysed, since the samples P1 and P5 only differ in the thermal oxide layer which does not interfere with the composition and structure of the catalyst external coat. The SEM images of the sample P1 are shown in Fig.26.

Fig.26. Scanning electron microscopy images of the morphology of the catalyst coat for different magnifications.

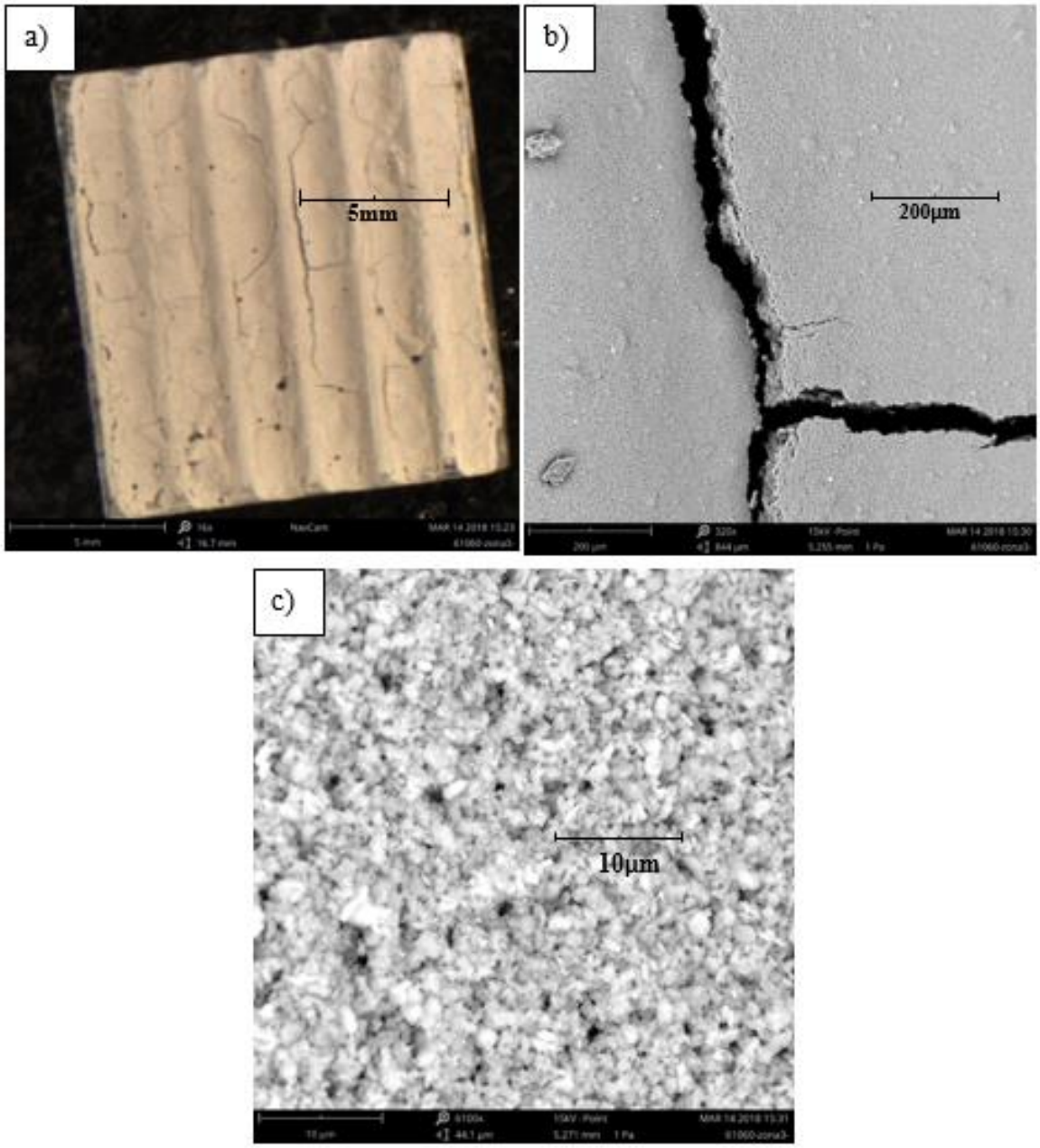

The catalyst coat appears uniform and only superficial crevasses occur, which suggest that the catalyst has been uniformly deposited. In these circumstances, the EDX is still necessary to check the catalyst coat composition. As always, the analyses were performed on 3 different random points shown on the Fig.27.

Fig.27. Placement of detection points, sample P1, catalyst deposited with water

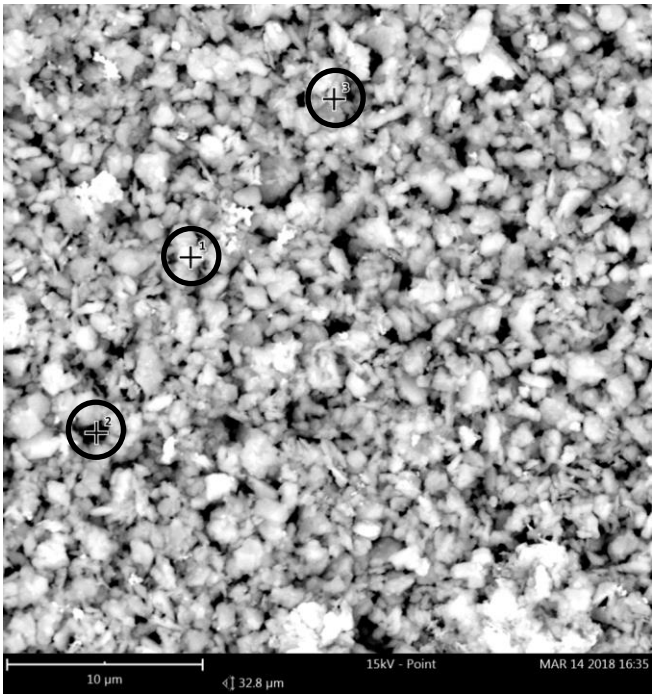

The spectra of the selected points are given on the Figs. 28, 29 and 30.

Fig.28. Spectrum and atomic-weight concentration, point 1, sample P1.

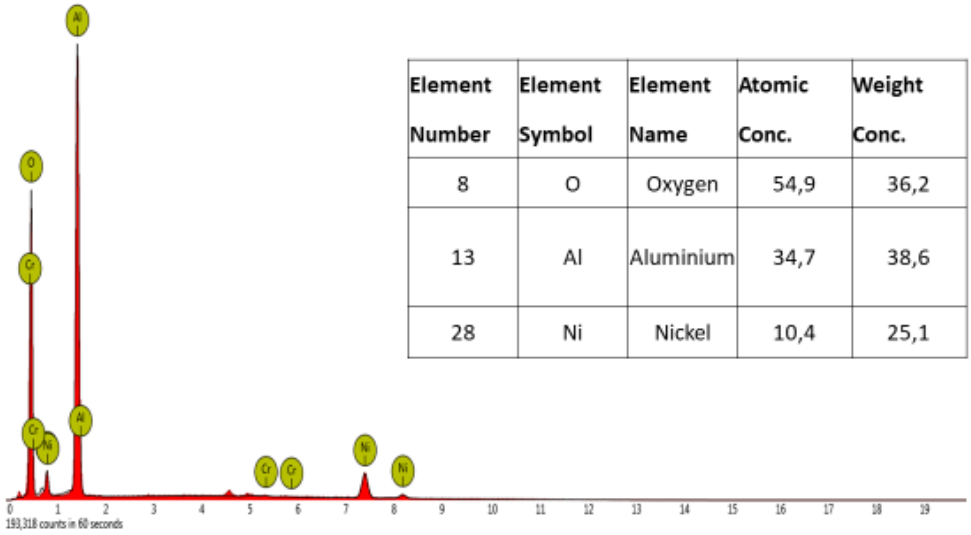

Element Number	Element Symbol	Element Name	Atomic Conc.	Weight Conc.
8	O	Oxygen	54,9	36,2
13	Al	Aluminium	34,7	38,6
28	Ni	Nickel	10,4	25,1

Fig.29. Spectrum and atomic-weight concentration, point 2, sample P1.

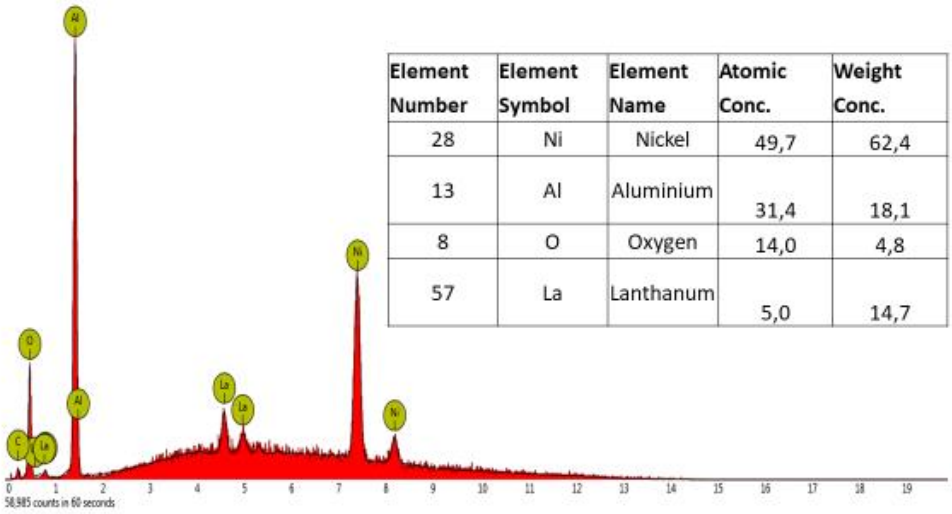

Element Number	Element Symbol	Element Name	Atomic Conc.	Weight Conc.
28	Ni	Nickel	49,7	62,4
13	Al	Aluminium	31,4	18,1
8	O	Oxygen	14,0	4,8
57	La	Lanthanum	5,0	14,7

Fig.30. Spectrum and atomic-weight concentration, point 3, sample P1.

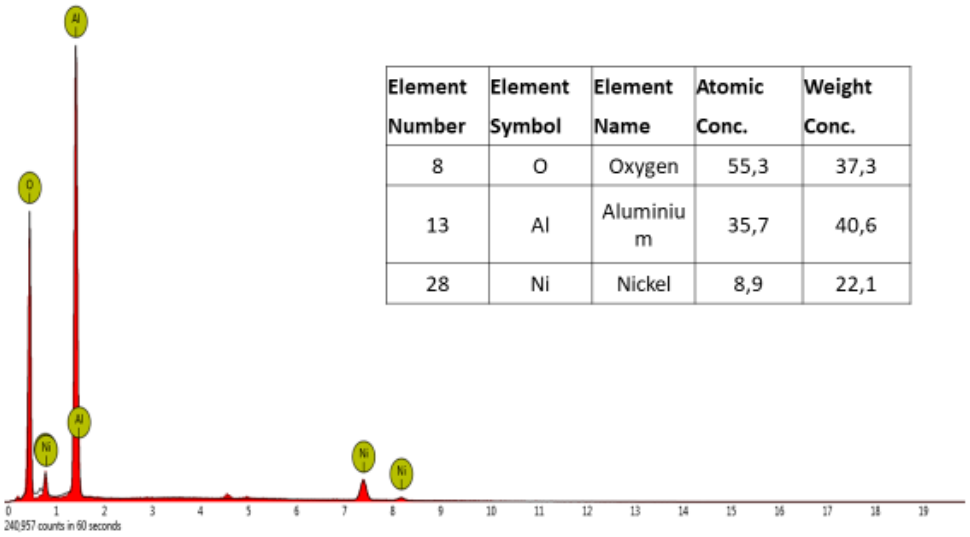

Element Number	Element Symbol	Element Name	Atomic Conc.	Weight Conc.
8	O	Oxygen	55,3	37,3
13	Al	Aluminium	35,7	40,6
28	Ni	Nickel	8,9	22,1

As it is shown from the spectra and the atomic concentrations, the catalyst is well distributed, and the active element (Nickel) is present in all three points.

In this connection, comparing the SEM-EDX analyses of the sample P1 and P2, it is possible to know which one has the best uniformity and elements distribution, and select the right method. Then, the SEM images are shown Fig.31.

Fig.31. Scanning electron microscopy images of the morphology of the catalyst coat for different magnifications. Catalyst deposited with PVA.

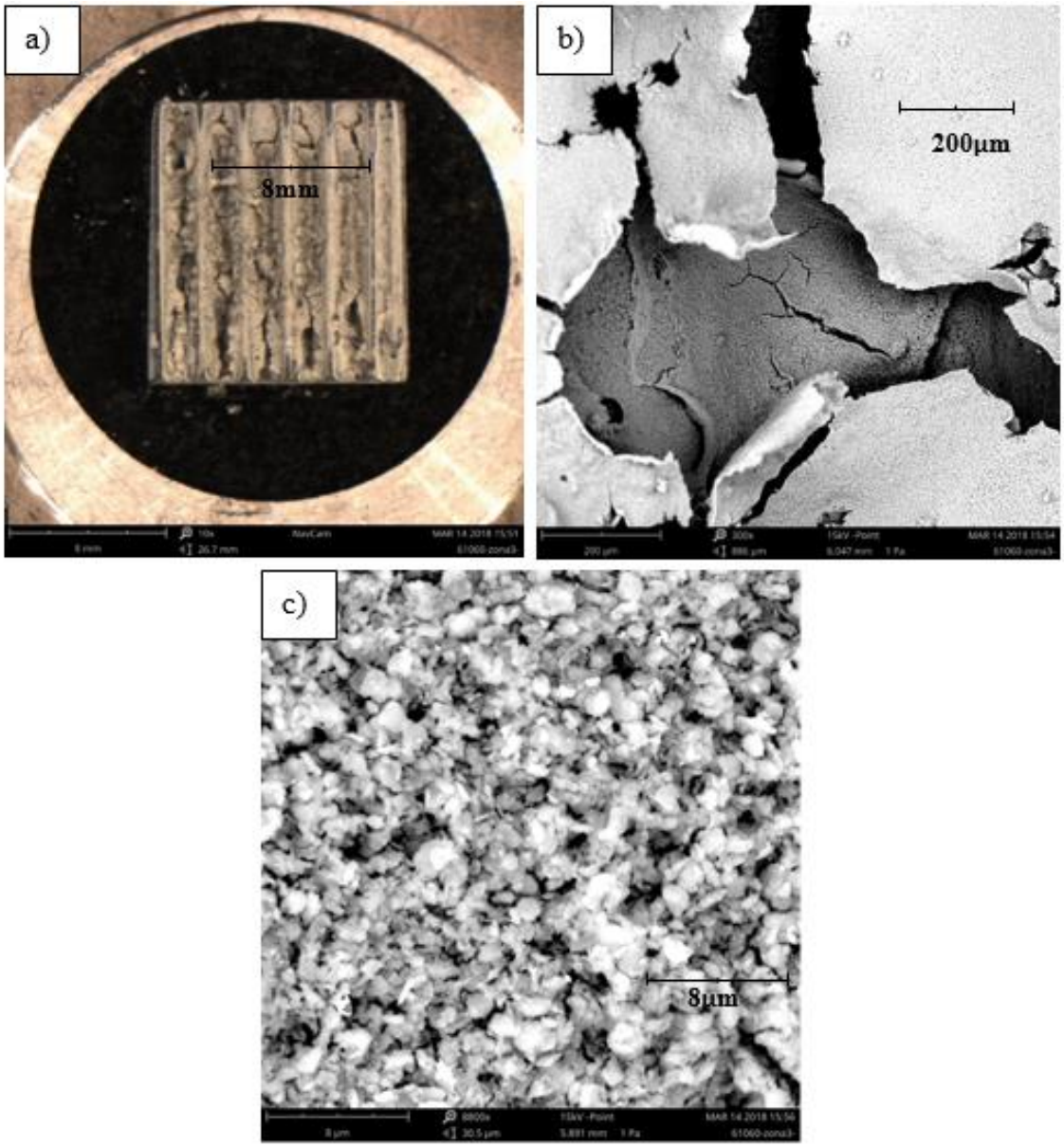

The catalyst layer of the sample P2 is not uniform as in the sample P1, many crusts and bobbles have formed on the surface, and this is more evident in the Fig.31 picture b). This issue could affect the mass transfer and the catalyst activity during the reforming, therefore the deposition with only water is preferred.

In addition, the spectra of three random points are reported in Figs.32, 33, 34 and 35 showing that the active phase, namely the Nickel, is not well distributed, and even absent in point 2. Furthermore, small amounts of chromium oxides of the metal plate are present, which did not appear in the sample P1 instead.

Fig.32 Placement of detection points, sample P2, catalyst deposited with PVA.

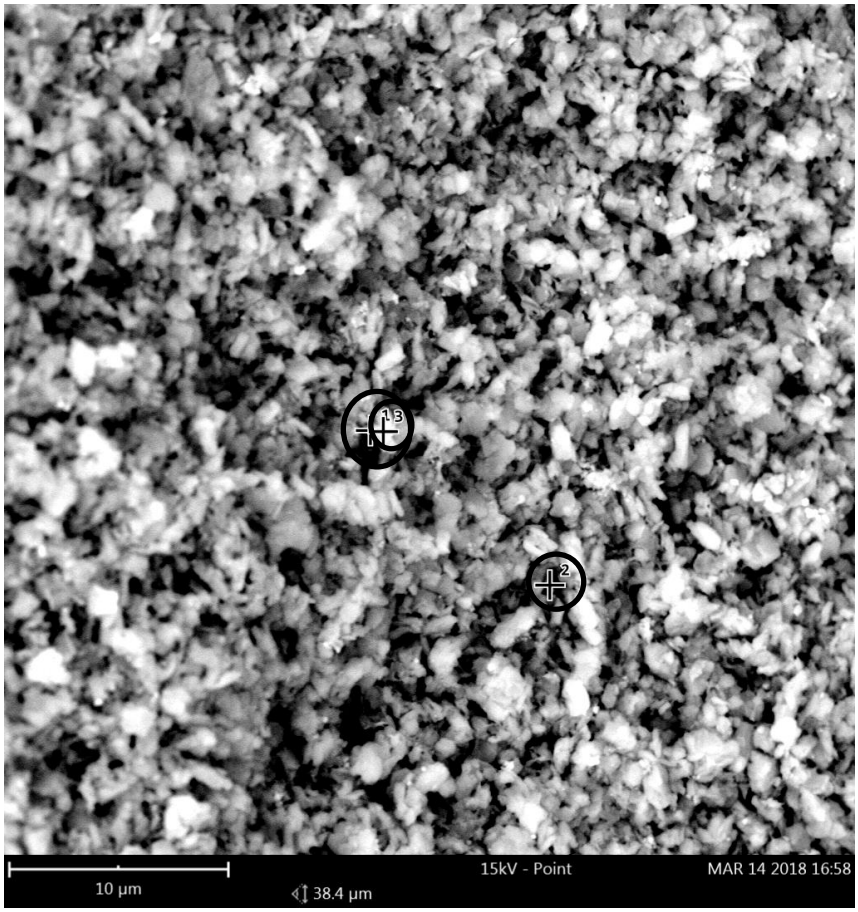

Fig.33. Spectrum and atomic-weight concentration, point 1, sample P2.

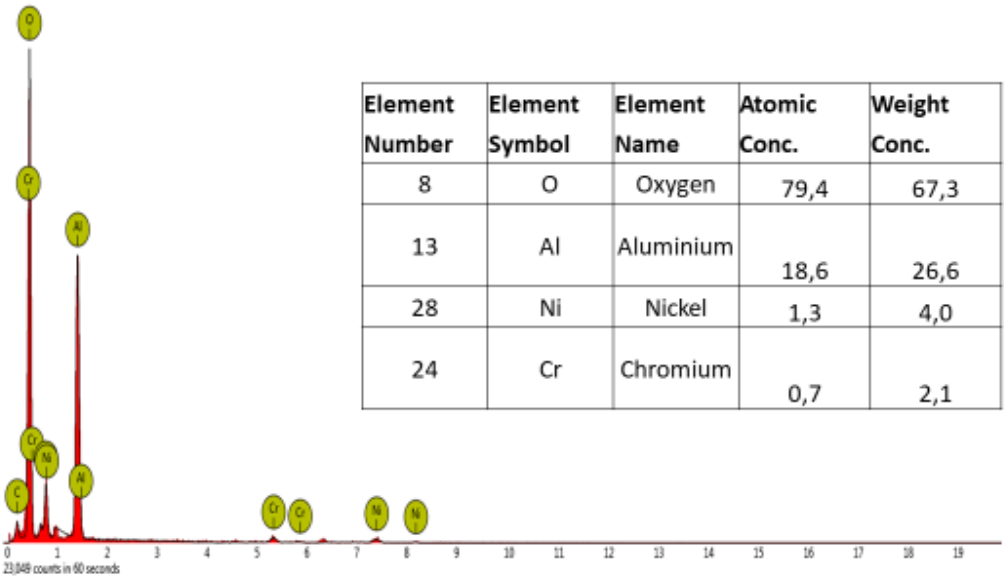

Element Number	Element Symbol	Element Name	Atomic Conc.	Weight Conc.
8	O	Oxygen	79,4	67,3
13	Al	Aluminium	18,6	26,6
28	Ni	Nickel	1,3	4,0
24	Cr	Chromium	0,7	2,1

Fig.34. Spectrum and atomic-weight concentration, point 2, sample P2

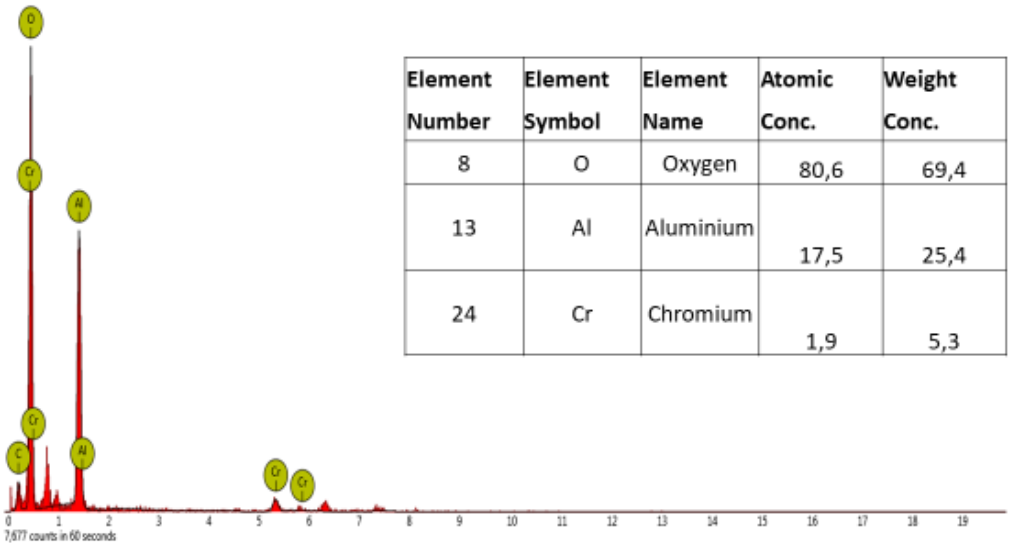

Element Number	Element Symbol	Element Name	Atomic Conc.	Weight Conc.
8	O	Oxygen	80,6	69,4
13	Al	Aluminium	17,5	25,4
24	Cr	Chromium	1,9	5,3

Fig.35. Spectrum and atomic-weight concentration point 3, sample P2

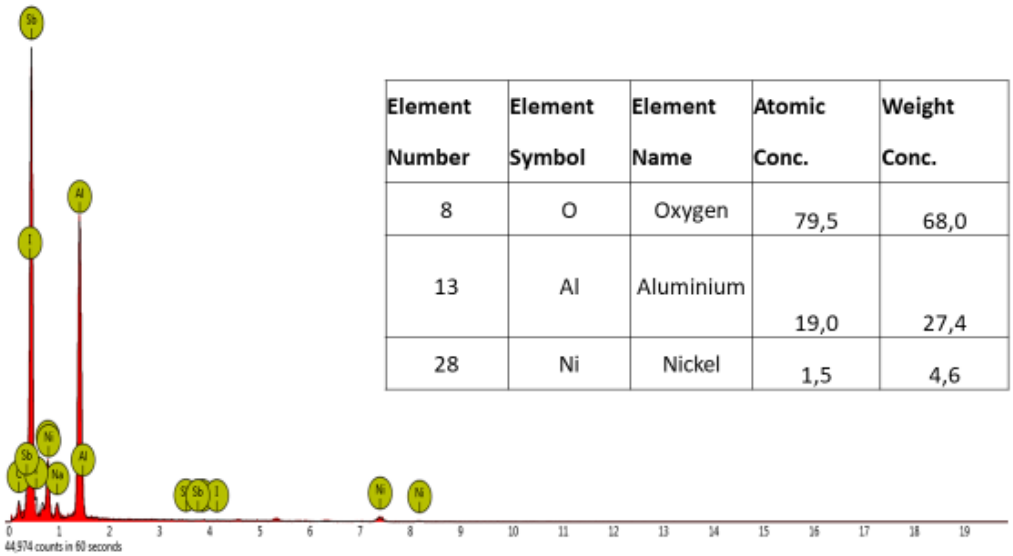

Element Number	Element Symbol	Element Name	Atomic Conc.	Weight Conc.
8	O	Oxygen	79,5	68,0
13	Al	Aluminium	19,0	27,4
28	Ni	Nickel	1,5	4,6

Thus, seeing the low amount of nickel in the surface, the impossibility to increase the amount of catalyst over 6 $\frac{mg}{cm^2}$ and the uniformity of the catalyst layer, which could affect the mass transfer during the reaction, the deposition with only water has been preferred to the one with polyvinyl alcohol.

4.5 Ultrasonic testing adherence.

After the catalyst deposition, an adherence's test has been carried out through ultrasonic waves. The samples P1, P2 and P5 has been placed in three different bakers with ethanol and then added on a ultrasonic cleaner for thirty seconds with a frequency of 37 kHz to observe the weight loss. A higher weight loss, therefore, means a weaker adherence between the catalyst and the plate's surface. Moreover, these conditions are very hard and for this reason, a high percentage of catalyst loss is expected.

So after the test, the milligrams of catalyst in samples P1, P2 and P5 are respectively 5 mg, 2 mg and 1 mg.

In the Fig.36 is shown the percentage of weight lost after the ultra-sonication.

Fig.36. % of weight loss after 30 seconds of ultra-sonication, sample P1,P2 and P5.

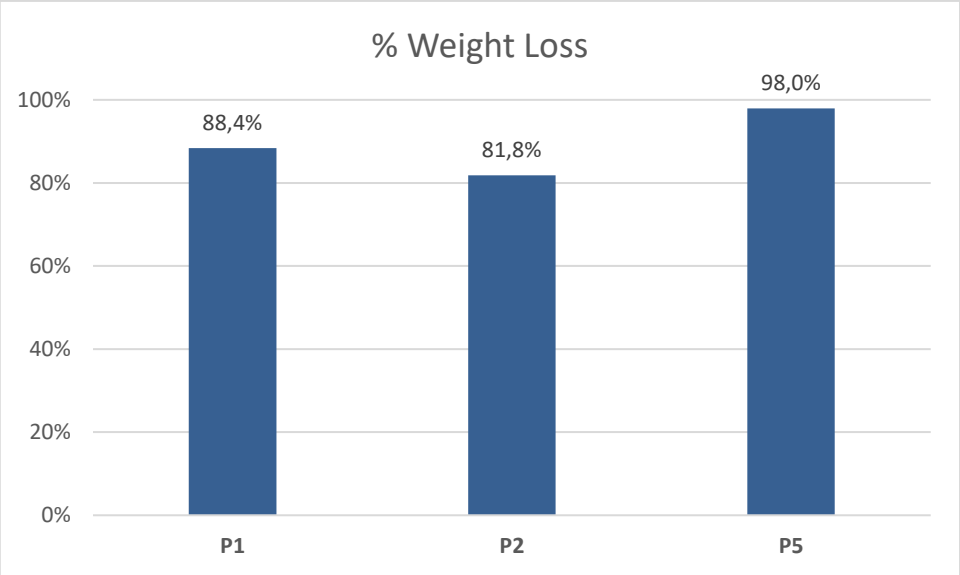

The best result is given by the sample P2 (81.8% of weight loss), the one where the catalyst has been deposited through PVA. However, for the reasons debated before, the slurry with only water has been chosen for the experiment. Moreover, from the results it is clear that the thermal pre-treatment is necessary to increase the catalyst adherence (10% higher) and thus the lifetime of the structured catalyst.

5. ADHERENCE' S IMPROVEMENT.

5.1 Introduction

As stated in the previous chapters, the good operation and the costs of maintaining of these kind of reactors are heavily dependent on the formation of an adherent support for the catalyst layer. It has already been seen the importance of the pre-treatment of the substrate, since the thermal one has improved the adhesion of the catalyst layer.

In most applications, alloys that containing aluminium are used, since Al_2O_3 is the oxide layer formed by thermal treatment, and it has a proven adherence and compatibility. Besides, in this application alumina is used as support for the catalyst.

V. Meille lists in a review all the methods used to form a thin layer of alumina to enhance the adherence of the subsequent washcoat in aluminium-free substrate (CVD, PVD, electrophoretic deposition) [26]. However, these techniques are expensive since they require complex machines.

For this reason, an easier method reported by Li Zhang [27] has been performed to find a better adhesion through an alumina coat.

5.2 Alumina Coat deposition

The slurry preparation consists on adding 2 wt. % of aluminium hydroxide powder to a 0,4 wt. % to HNO_3 aqueous solution, and the control the pH value until 3.5. Then, the boehmite sol is mixed with the 4 wt. % PVA and stirred for 2 h and results in alumina sol. In this work, three samples have been prepared to test the alumina coat, and called P8, P9 and P10. The plates have been set to test an application with PVA and previous thermal treatment, one without PVA, and the last without PVA and thermal treatment. To a have a better overview, the testing condition are summarized in Table 6.

Tab.6. P8, P9, P10. Samples features.

	Thermal pre-treatment	**Slurry coat composition**
P8	Yes	4 wt. % PVA, 2 wt. % $Al(OH)_3$, 0,4 wt. % HNO_3
P9	No	4 wt. % PVA, 2 wt. % $Al(OH)_3$, 0,4 wt. % HNO_3
P10	Yes	2 wt. % $Al(OH)_3$, 0,4 wt. % HNO_3

Once the slurry has been prepared, it has been put in the micro-channels thanks to a syringe of the same model used for the catalyst filling. Then, the plates have been dried at room temperature for 3 hours and after in a hoven at 120°C for 8 h. Once finished this step, they have been calcined at 600°C for 5 hours with a ramp of 2 $\frac{^{\circ}C}{min}$. The Fig.37 shows how the samples appear after deposition.

Fig.37. Samples P8, P9 and P10 after alumina coat deposition.

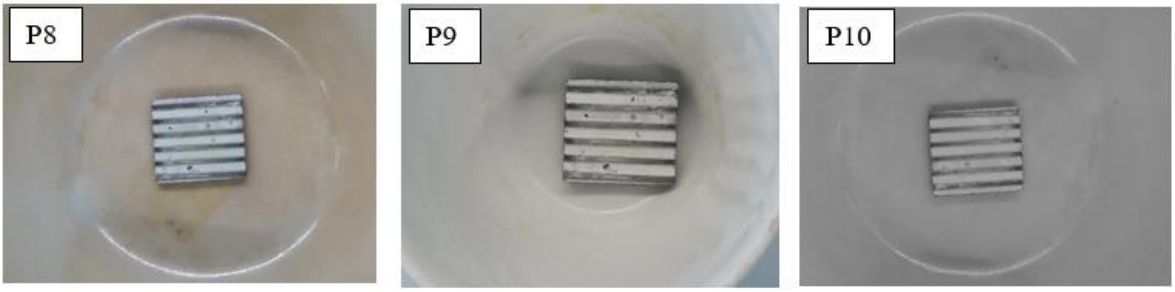

The alumina layer deposited on the Sample P8 is 2 mg, 3 mg on the P9 and 2 mg on the P10.

5.2 Catalyst deposition

The catalyst has been added in the micro-channel in the way that was seen to be the best in chapter 4.4, namely the slurry composed with only water and catalyst. The only difference here is that the deposition's process has been repeated only one time to make sure that the catalyst layer

does not interfere with the plates inside the metal cylindrical block. Therefore, after the calcination at 400 °C, the catalyst has been set on the plate, and the samples weight are reported in Table 7.

Tab.7. Final summary after catalyst deposition.

	Plate weight (g)	Alumina layer weight (mg)	Catalyst weight (mg)	$\frac{mg\ of\ catalyst}{cm^2}$
P8	2,694	2	8	4,0
P9	2,783	3	6	3,0
P10	2,760	2	6	3,0

5.3 Ultrasonic testing adherence

The ultrasonic test has been carried out for the three samples in order to compare the catalyst layer adherence with alumina to the one without. For this reason, the testing conditions are the same as describe above in chapter 4.5. , which means thirty seconds with a frequency of 37 kHz in a baker full of ethanol.

At the end of the test, the weight loss, which represents a measure of the adhesion of the catalyst coat, is reported on Table 8 and in the Fig.38 are shown the plates.

Tab.8. Ultrasonic test adherence results.

	Weight of catalyst after ultra-sonication	Percentage of weight lost
P8	1 mg	88,7%
P9	1 mg	83,3%
P10	4 mg	33,3%

Fig.38. Plates P8, P9, and P10 after the ultrasonic test.

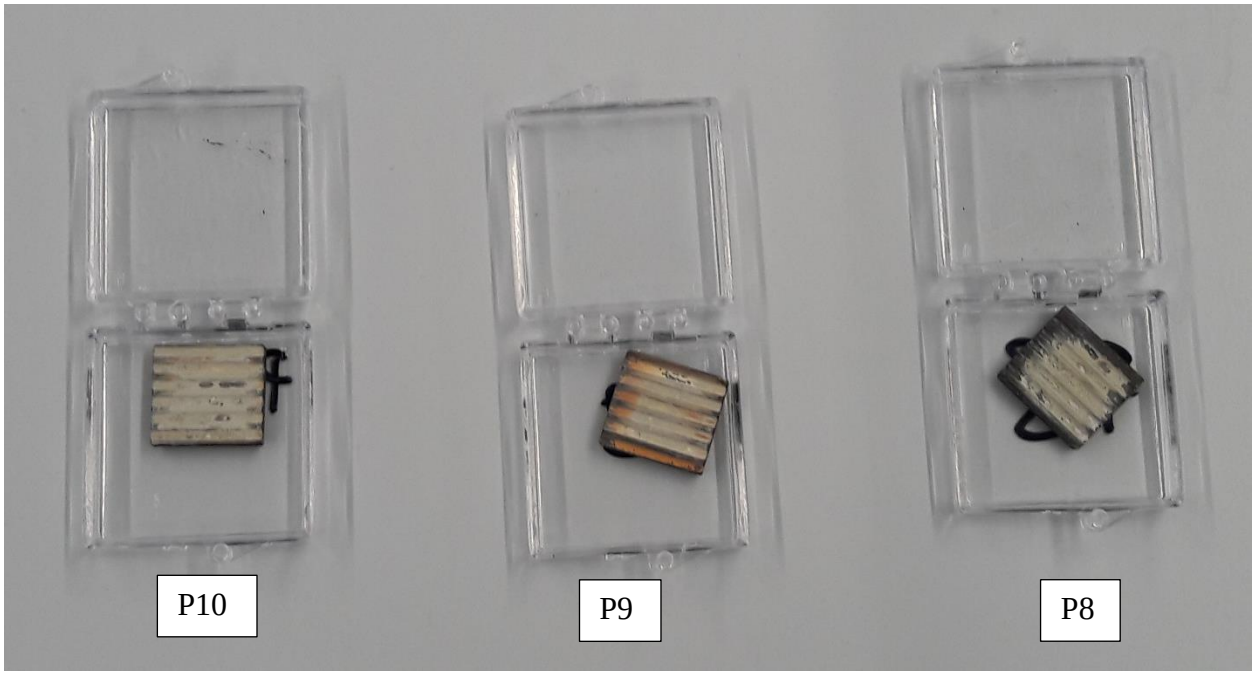

As is shown, the sample P10, the one in which the PVA has not been used, and that has been treated thermally, has by far the best result. In the histogram of Fig.39 it is clear that all the samples reach the same achievement more or less, both with alumina and without, except for the sample P10, namely the one with the chromium oxide layer and a an alumina intermediate layer deposited without the aid of PVA.

Fig.39. Percentage of weight loss after 30 seconds of ultra-sonication, effect of the alumina layer on the adherence. Comparison between P1, P2, P5 and P8, P9 and P10.

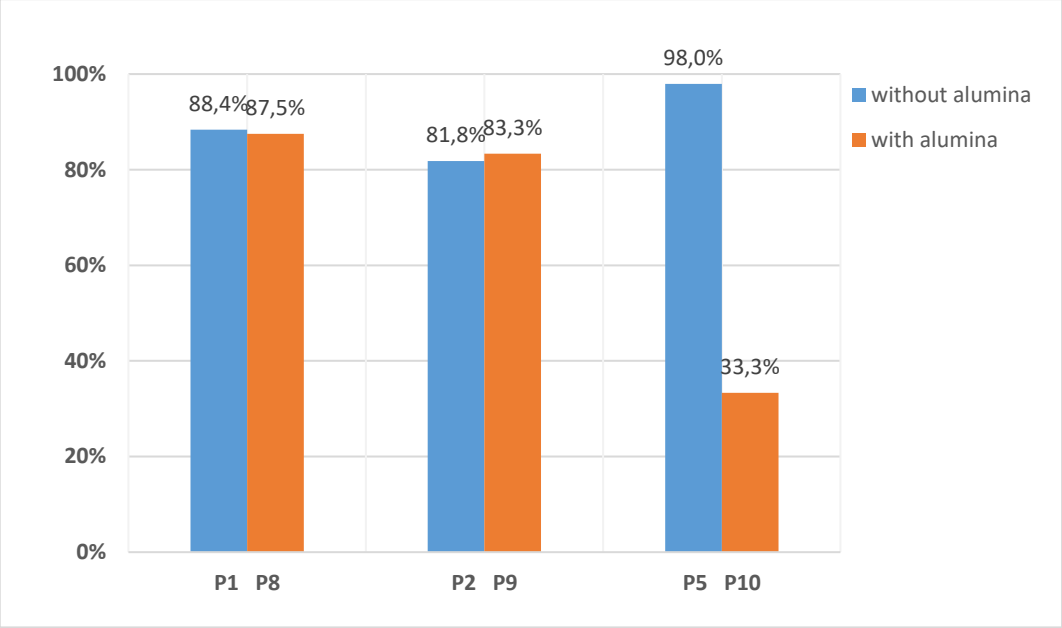

The good performance achieved with the sample P10 is probably due to the better diffusion of the alumina layer in the chromium oxide attributable to the increasing of the temperature of calcination (400 °C against 600 °C) and also for the better interaction between the catalyst and the alumina. For this reason, this last configuration has been chosen to test the reaction.

6. STEAM REFORMING TEST ON CORDIERITE MONOLITHIC REACTOR

6.1 Steam reforming set-up and testing conditions.

The schematic diagram of the set-up for the experimentation and a photo of it are respectively shown in Figs.40 and 41.

Fig.40. Experimental set-up diagram for steam reforming test.

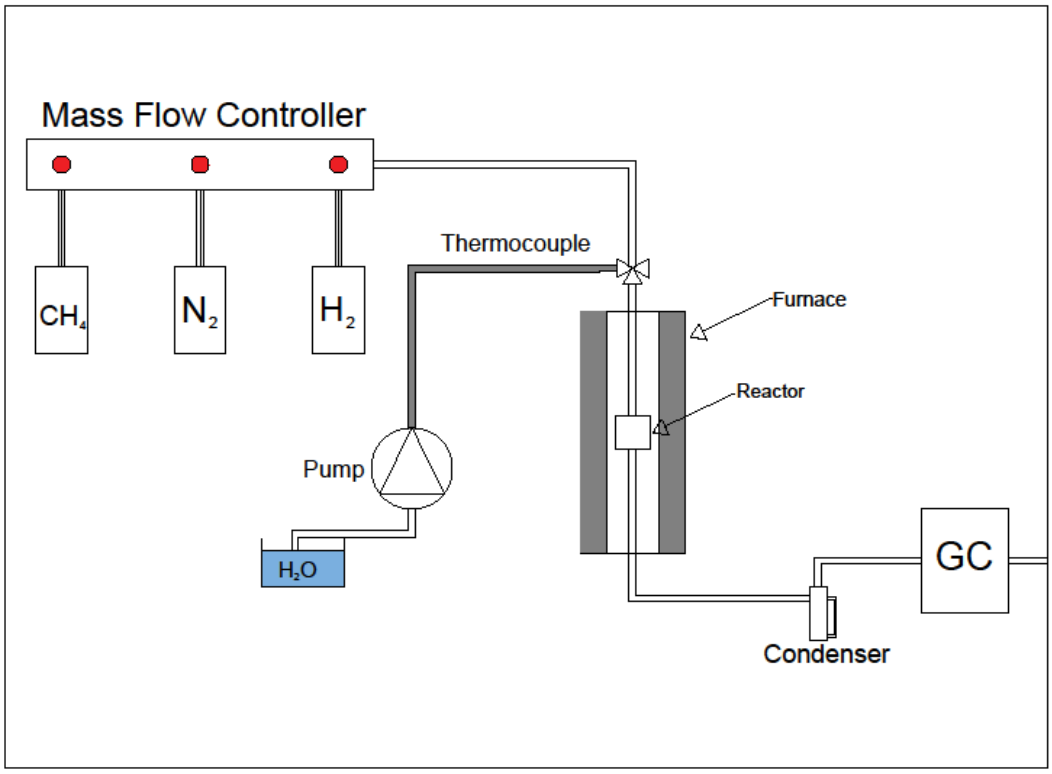

Fig.41. Experimental set-up photo.

The plant consists of a mass flow control, which monitors the flow of the gaseous reactants, a furnace, the aim of which is to maintain the reaction temperature, a pump linked with a thermocouple at 130 °C in order to inject the steam, and at the end a condenser, before sending the flow to the gas chromatography.

Considering the different geometrical, spatial and chemical configurations of the cordierite reactor and of the micro-structured one, it is crucial that the testing condition are set in such a way that the performances of the two reactors are comparable. For this reason, since the cordierite reactor holds a higher amount of catalyst inside, it has been decided to always work with the same ratio between gases inlet flow and milligrams of catalyst (F/W). The ratios used are 0.2, 0.6, 0.8 and 1.4 $\frac{mL\ of\ inlet\ gas}{mg\ of\ catalys \cdot\ min}$. The others working condition are reported on Tab.9.

Tab.9. Working condition for the reactor's test.

Temperature	800 °C
Pressure	1 bar
Steam carbon (S/C) ratio	2

Considering the monolith A1, it contains 571 mg of catalyst inside, so in Tab.10 are shown the values of the flows of methane and steam for the different ratios and gas hourly space velocity (GHSV) calculated considering a volume of 3,12 mL.

Tab.10. Gases inlet flow and GHSV calculated for the reactor A1.

$\frac{mL\ of\ inlet\ gases}{mg\ of\ catalys\ \cdot\ min}$	$\frac{mL\ of\ inlet\ gases}{min}$	GHSV h^{-1}
0,2	114,2	2196
0,6	342,6	6588
1	571	10980
1,4	799,4	15373

Before proceeding with the reaction, the methane mass flow controller and the pump have been calibrated manually. The calibration curves are shown in Figs.42 and 43 for the mass flow and in Fig.44 for the pump.

Fig.42. Calibration curve for methane mass flow controller in the range 11-18 mL/min of real flow.

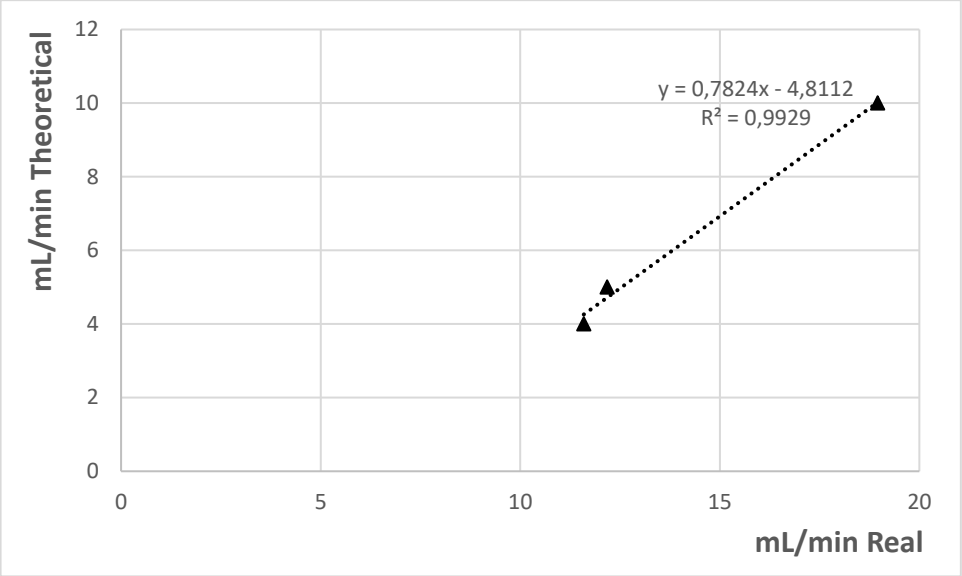

Fig.43. Calibration curve for methane mass flow controller in the range 23-52 mL/min of real flow.

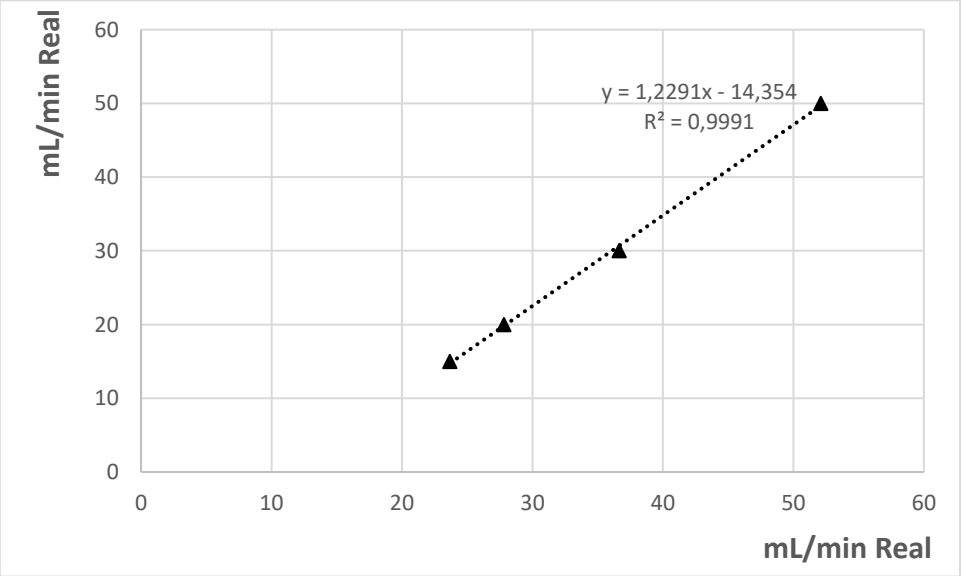

Fig.44. Calibration curve for the pump.

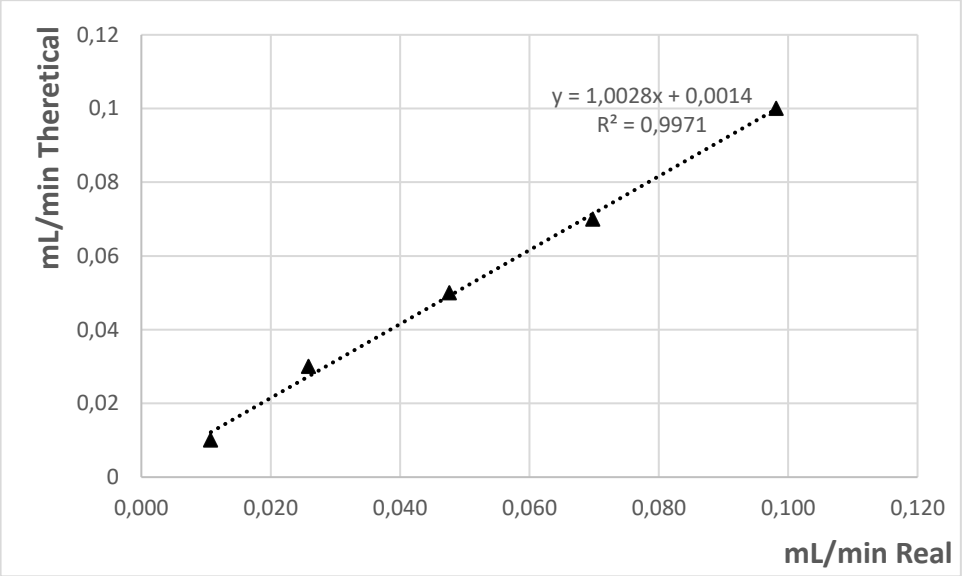

6.2 Steam reforming test results.

Before proceeding with the reaction, the pre-treatment consisting of reduction and aging must be carried out. This pre-treatment is essential to reduce the Nickel oxide into the active particles of Ni.

The activation by reduction of the catalyst is performed before the reaction's test, for both type of reactor on mixture of 20% of H_2 in N_2, with a total flow of 100 $\frac{mL}{min}$ from ambient temperature up to 800°C, working with a ramp of $\frac{5°C}{min}$. When the ramp is over, the reducing condition must be maintained for one hour. After that, it continues with the aging, changing the inlet flow with a mixture of $H_2{:}H_2O = 1:3$. The H_2 flow is 10 $\frac{mL}{min}$, and then, we can introduce 10 $\frac{mL}{min}$ of carrier gas (N_2). At the end, we let it age with the same mixture for 1,5 hours at 800 °C. The purpose is to treat the catalytic device badly to simulate hard working conditions.

The reaction has been conducted for an hour for each ratio flow/mass of catalyst, but the it was not possible to perform the ratio of 1,4 $\frac{mL\ of\ inlet\ gases}{mg\ of\ catalys \cdot\ min}$ because it exceeds the maximum capacity limit of the mass flow controller.

Then, the data collected by the gas chromatograph has been acquired and analysed. The first parameter calculated and considered is the percentage of methane converted into the product gases. The Figs.45, 46, 47, and 48 show the conversion as time goes on for the three different ratio mL of inlet gases/min/mg of catalyst.

Fig. 45 Methane conversion, 0,2 $\frac{mL\ of\ inlet\ gases}{mg\ of\ catalys \cdot\ min}$.

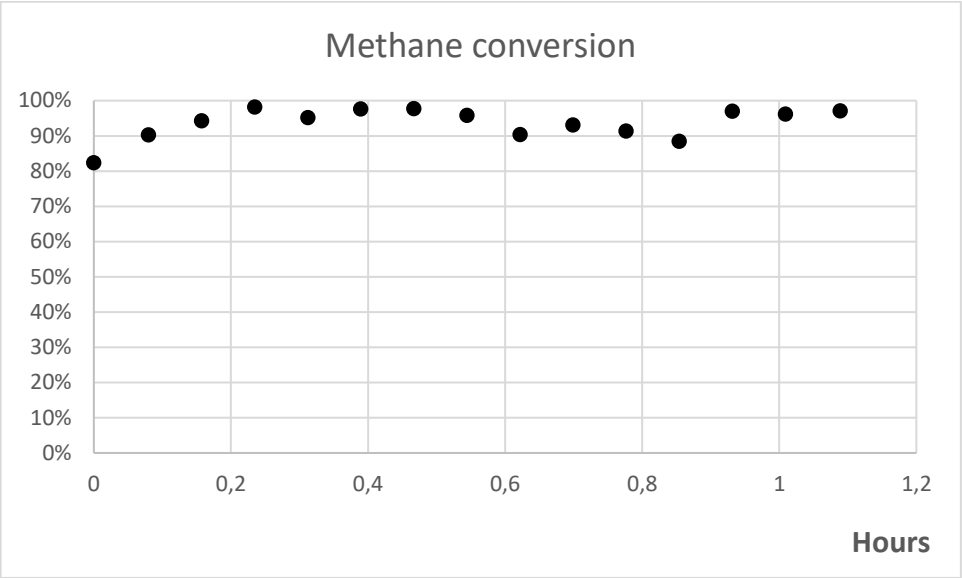

Fig.46. Methane conversion, 0,6 $\frac{mL\ of\ inlet\ gases}{mg\ of\ catalys \cdot\ min}$.

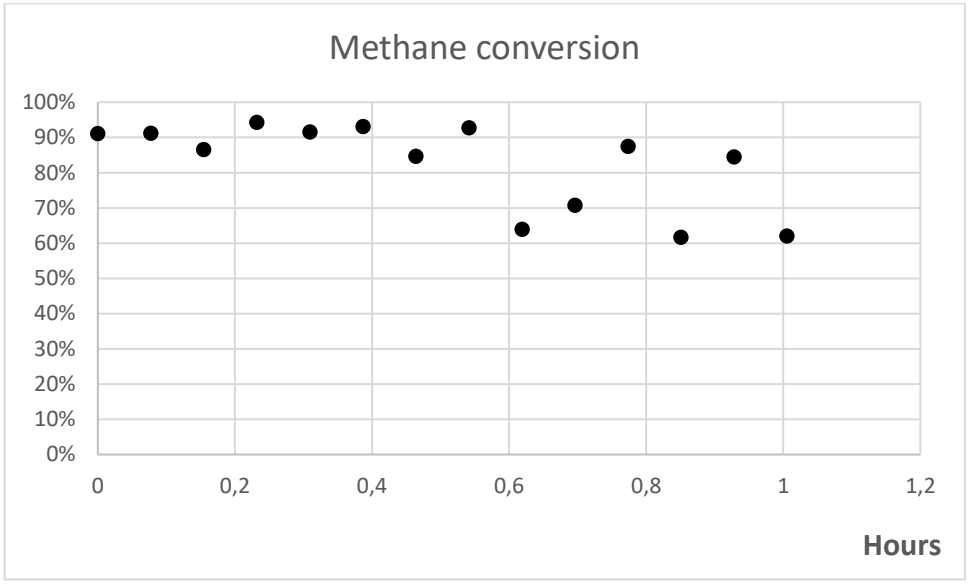

Fig.47. Methane conversion, 1 $\frac{mL\ of\ inlet\ gases}{mg\ of\ catalys \cdot\ min}$.

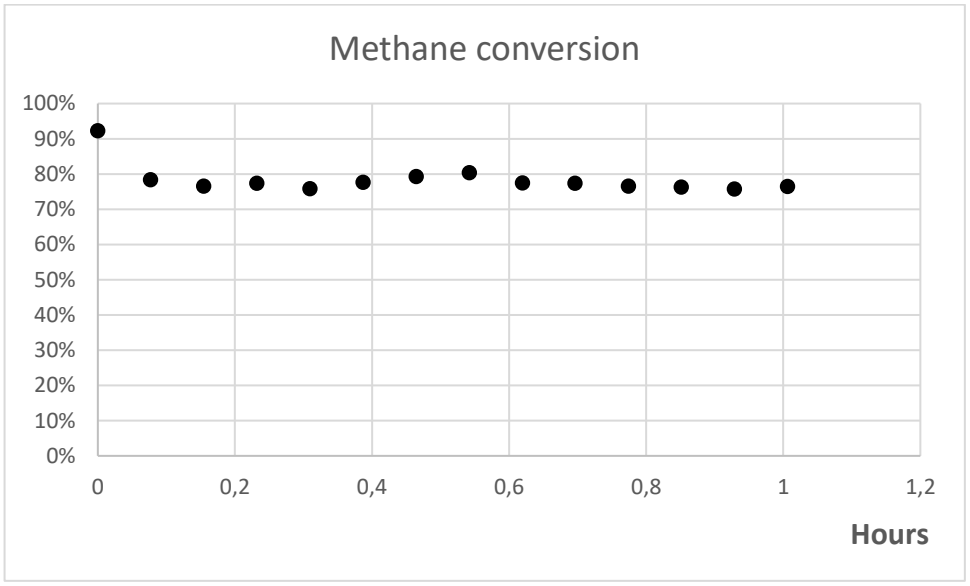

Fig.48. Methane conversion comparison.

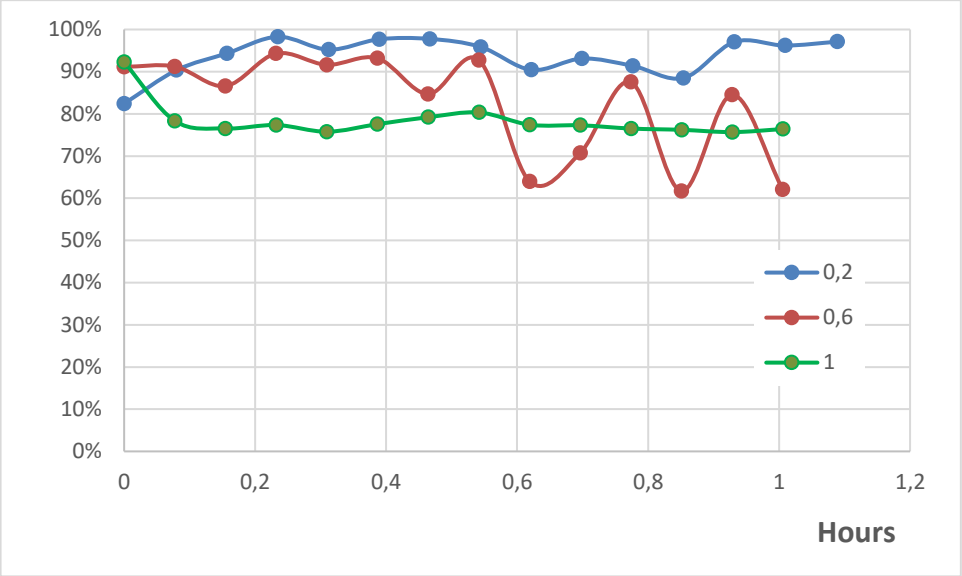

Thanks to the high geometrical surface area, the cordierite monolith is able to convert a high percentage of methane, as has already been known. In particular, it is possible to reach a conversion around 94% with a flow of 114,2 $\frac{mL}{min}$ of gases. However, increasing the flow, the mass transfer is no longer optimized and the catalyst begins to undergo the fouling process, so the conversion decreases.

The Nickel based catalysts are more subjected to the risk of carbon formation, even if higher hydrocarbons are more prone than methane.

Rostrup-Nielsen [7] identify three routes of carbon formation on nickel surface. In this case, the one at high temperature is interested and it involves the formation of whisker carbon.

Analysing the conversion into a single series time, this is easily observable (Fig.49).

Fig.49. Methane conversion along the time.

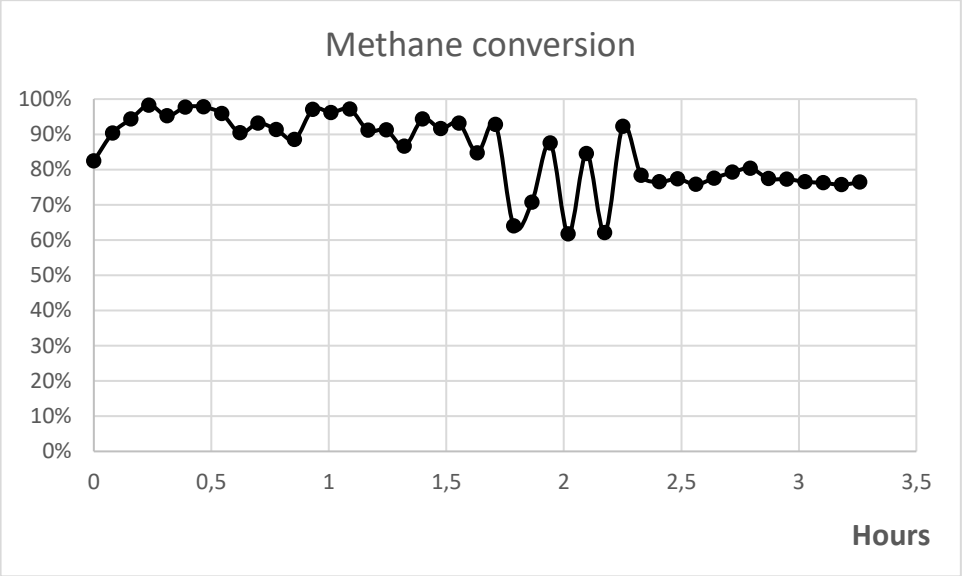

The carbon deposition on the catalyst can also be observed from the trend of production or selectivity of carbon oxides. Remembering that carbon is usually considered the product of CO disproportionation ($2CO \rightarrow C + CO_2$), the trends on Figs.50, 51, and 52 confirm what has been said, since they show an increase in carbon dioxide production when the methane conversion decrease, sign that then the catalyst is deactivating.

Fig.50. Carbon oxides production trends, 0.2 $\frac{mL\ of\ inlet\ gases}{mg\ of\ catalys \cdot\ min}$.

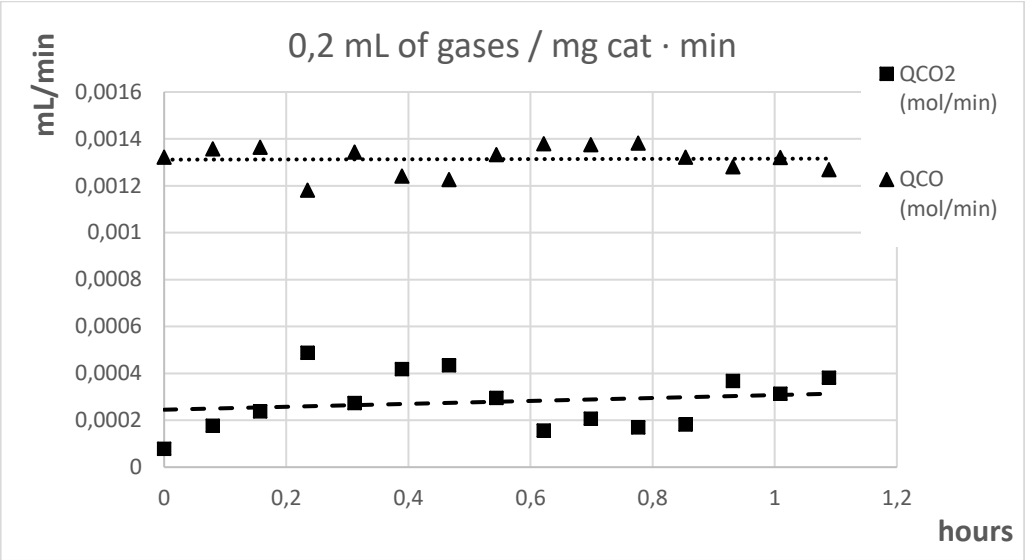

Fig.51. Carbon oxides production trends, 0.6 $\frac{mL\ of\ inlet\ gases}{mg\ of\ catalys \cdot\ min}$.

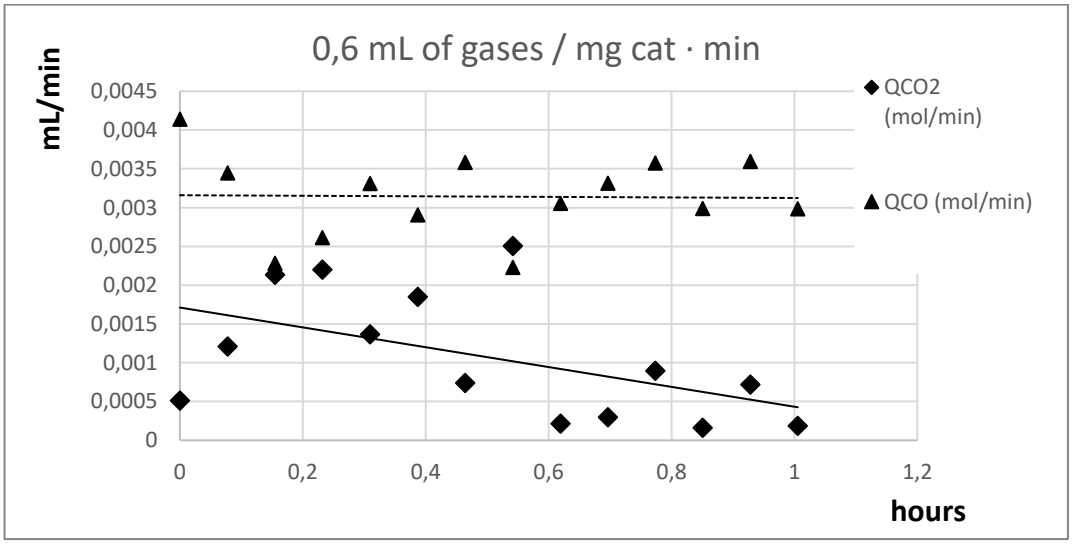

Fig.52. Carbon oxides production trends, 1 $\frac{mL\ of\ inlet\ gases}{mg\ of\ catalys \cdot min}$.

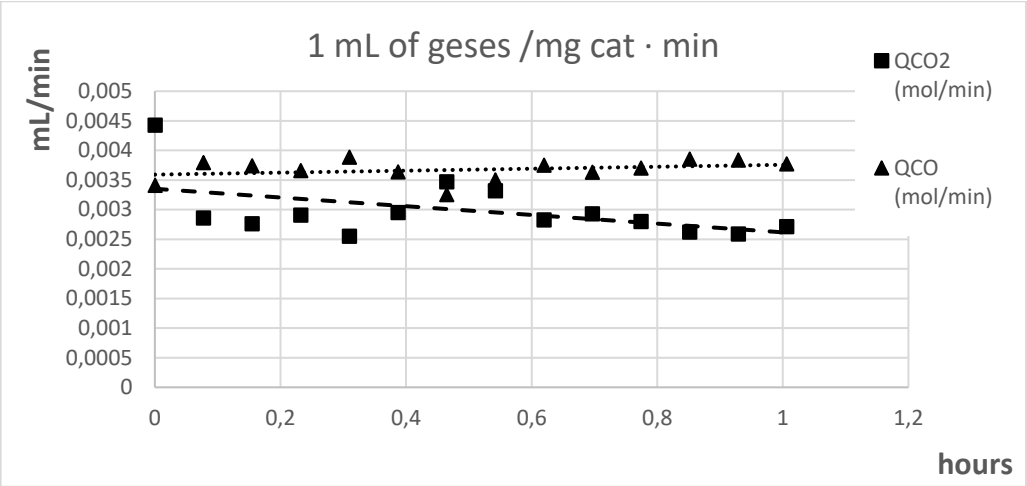

Fig.53. Selectivity of reaction products.

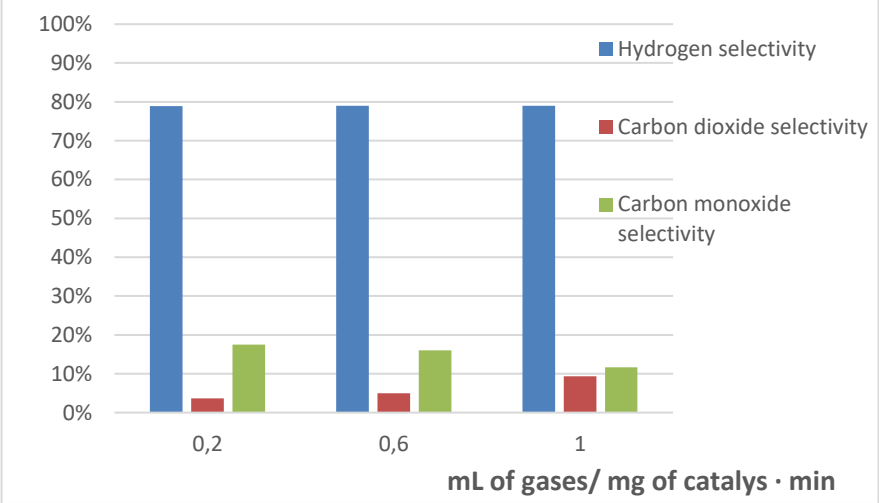

In addition to deactivation, carbon deposits can grow so large that they can cause total blockage of the reformer tubes.

Regarding hydrogen production, the selectivity remains constant and therefore increasing the flow of inlet gases, the outlet hydrogen flow increases (Fig.54).

Fig.54. Hydrogen production.

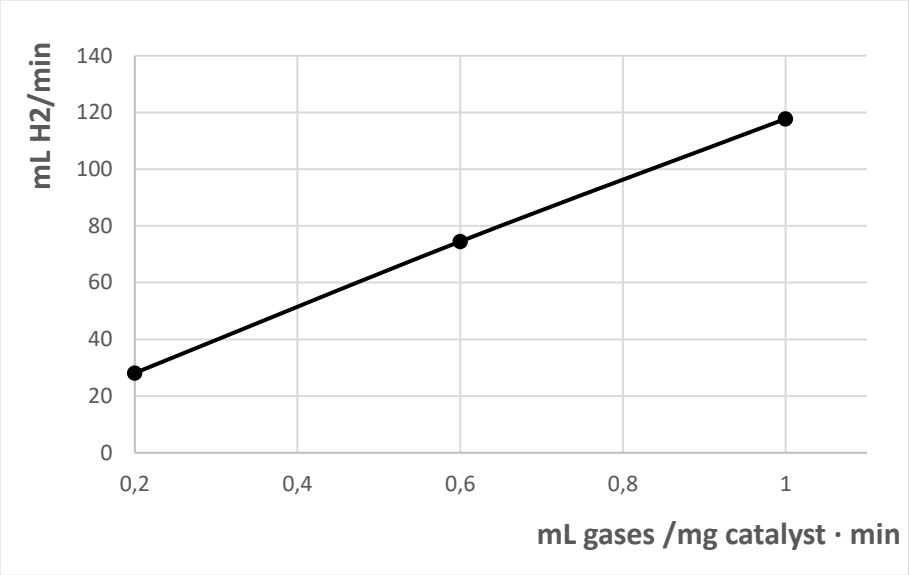

7. STEAM METHANE REFORMING ON MICRO-STRUCTURED REACTOR.

7.1 Testing conditions

Once it was seen that the configuration with the alumina layer was the best, the reactor has been prepared for the test following the method described in the chapter 5.2. A total of 64 mg of catalyst has been put on the metal plates, with an average of 4,5 $\frac{mg\ of\ catalyst}{cm^2}$ for each plate.
The working conditions are the same of the Tab.9 for the cordierite monolith, with the same temperature, pressure and steam to carbon ratio. Instead, the amount of inlet flow rate changes, since the weight of catalyst is different and the proportion between flow and catalyst must be kept constant (0.2, 0.6, 1, 1,4 $\frac{mL\ of\ inlet\ gases}{mg\ of\ catalys\cdot\ min}$). The millilitres per minute and the gas space velocity have been calculated and are reported on Tab.11.

Tab.11 Gases inlet flow and GHSV calculated.

$\frac{mL\ of\ inlet\ gases}{mg\ of\ catalys\ \cdot\ min}$	$\frac{mL\ of\ inlet\ gases}{min}$	GHSV h^{-1}
0,2	12,8	1875
0,6	38,4	5626
1	64	9377
1,4	89,6	13128

Unfortunately, it was not possible to test the reaction with 12,8 $\frac{mL\ of\ inlet\ gas}{min}$, because this value exceeds the minimum flow rate of the mass flow controller.

7.2 Steam reforming test results.

The first graphs shown are related to the conversion of methane (Figs. 55, 56 and 57) for the different ratios flow / weight of catalyst.

Fig.55 Methane conversion, 0,6 $\frac{mL\ of\ inlet\ gases}{mg\ of\ catalys \cdot\ min}$.

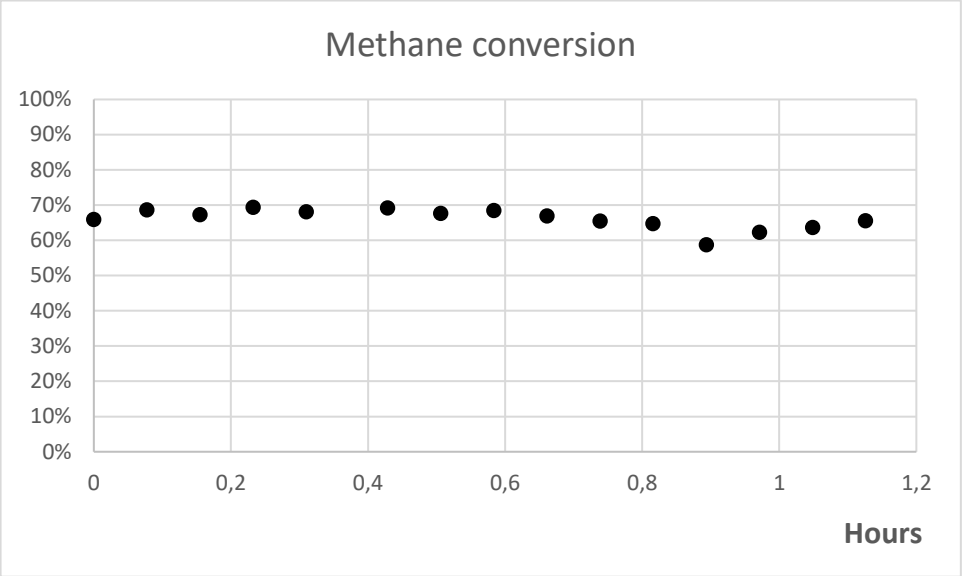

Fig.56. Methane conversion, 1 $\frac{mL\ of\ inlet\ gases}{mg\ of\ catalys \cdot\ min}$.

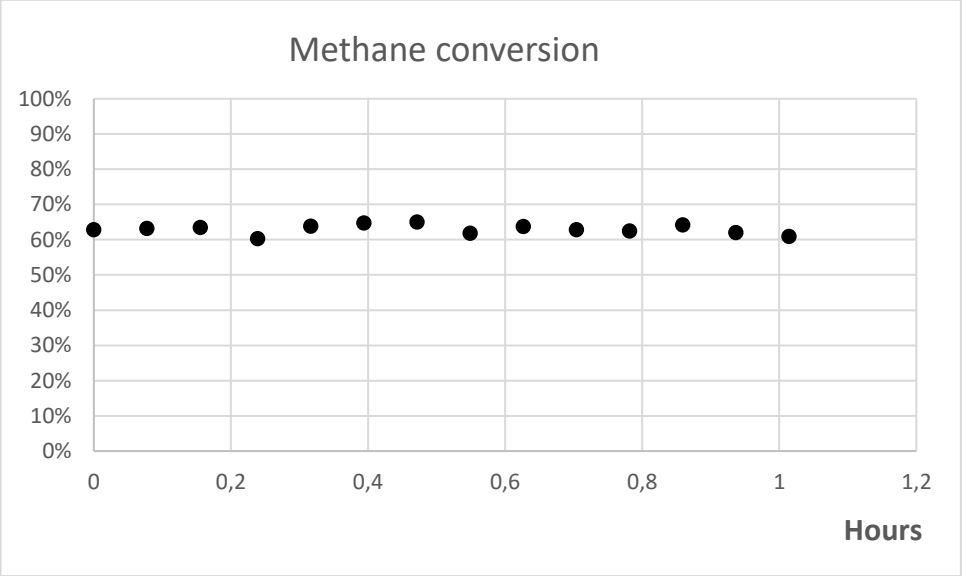

Fig.57 Methane conversion, 1,4 $\frac{mL\ of\ inlet\ gases}{mg\ of\ catalys \cdot\ min}$.

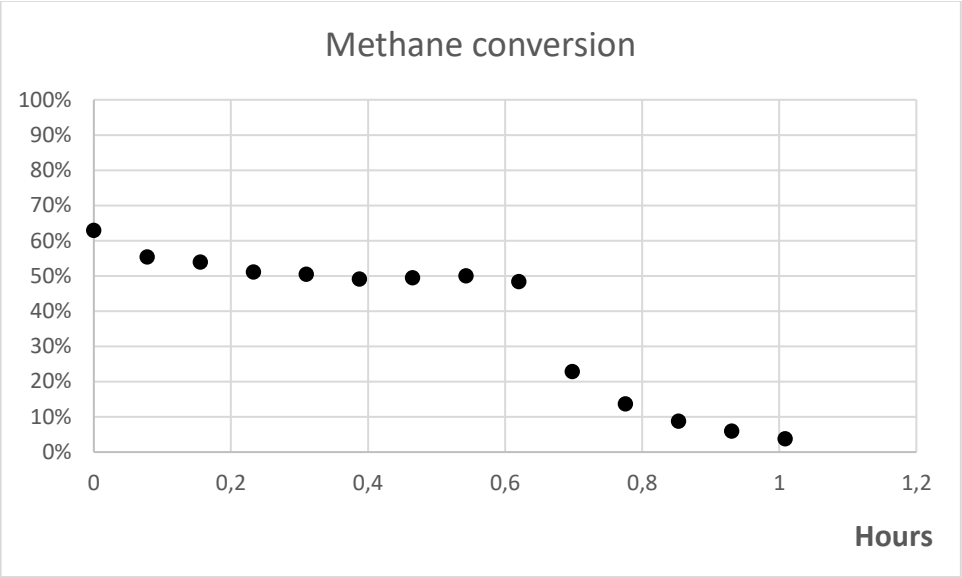

Fig.58. Methane conversion comparison.

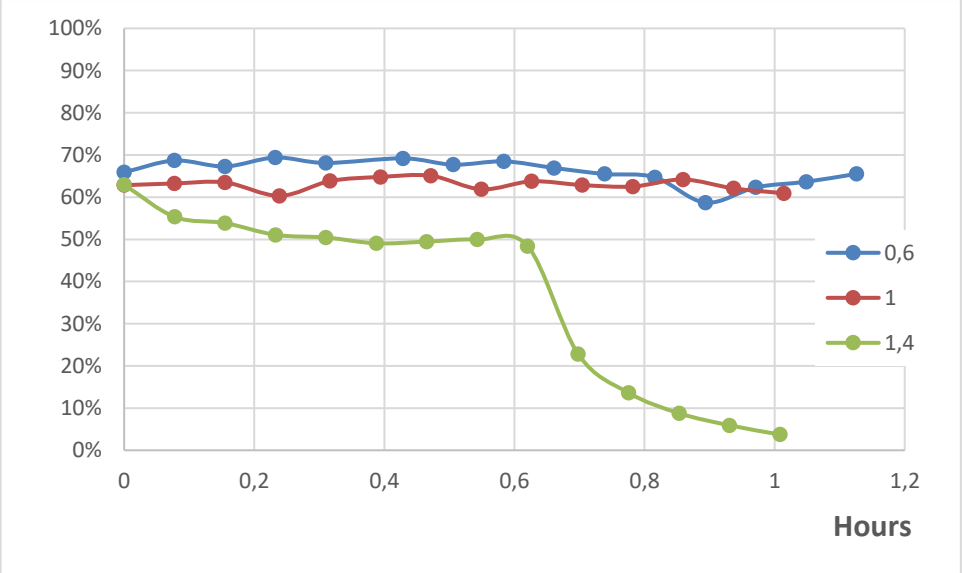

When the reaction is working with the lowest flow ($0.6\frac{mL\ of\ inlet\ gases}{mg\ of\ catalys \cdot\ min}$) the methane conversion reaches its maximum point, which is around 65-70%, then it decrease both for the mass transfer which becomes more complicated, and for the fouling.

The fouling process is clearly observed in the graph of Fig.58 it is possible to observe a rapidly declining of the methane conversion, sign that the catalyst is deactivating.

The following Figs. 59, 60 and 61 show the distribution of carbon oxides for the different F/W ratios.

Fig.59.. Carbon dioxide and monoxide production, $0,6\frac{mL\ of\ inlet\ gases}{mg\ of\ catalys \cdot\ min}$.

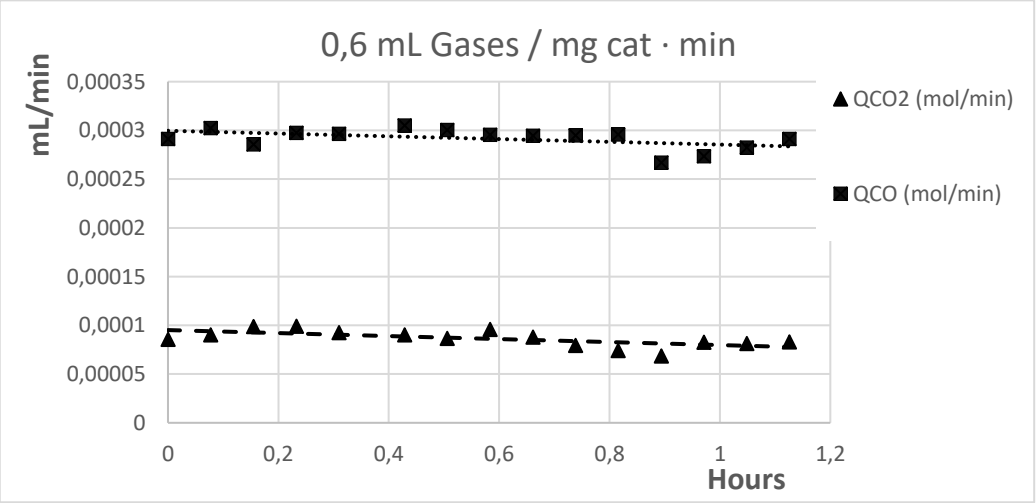

Fig.60. Carbon dioxide and monoxide production, 1 $\frac{mL\ of\ inlet\ gases}{mg\ of\ catalys \cdot\ min}$.

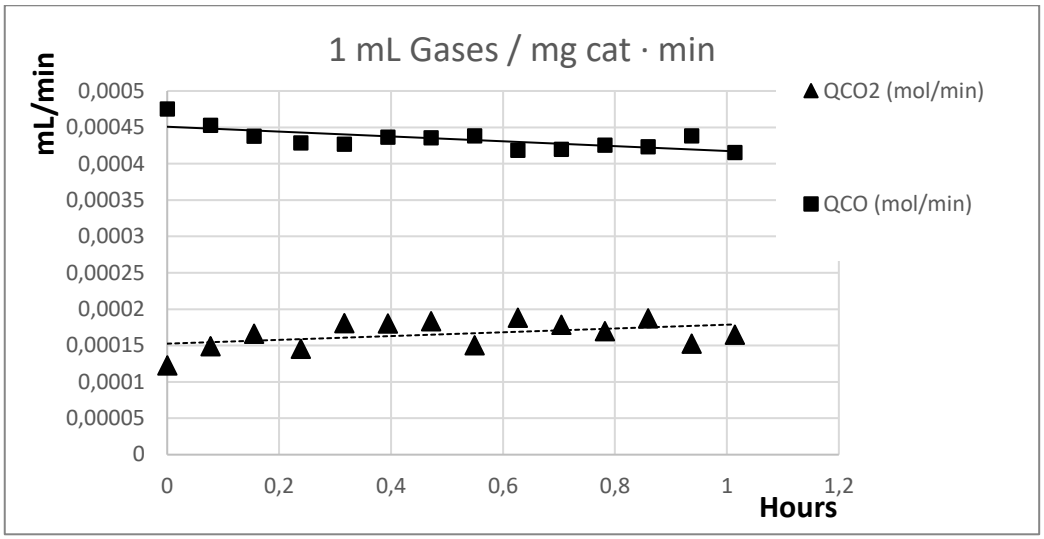

Fig.61. Carbon dioxide and monoxide production, 1.4 $\frac{mL\ of\ inlet\ gas}{mg\ of\ catalys \cdot\ min}$.

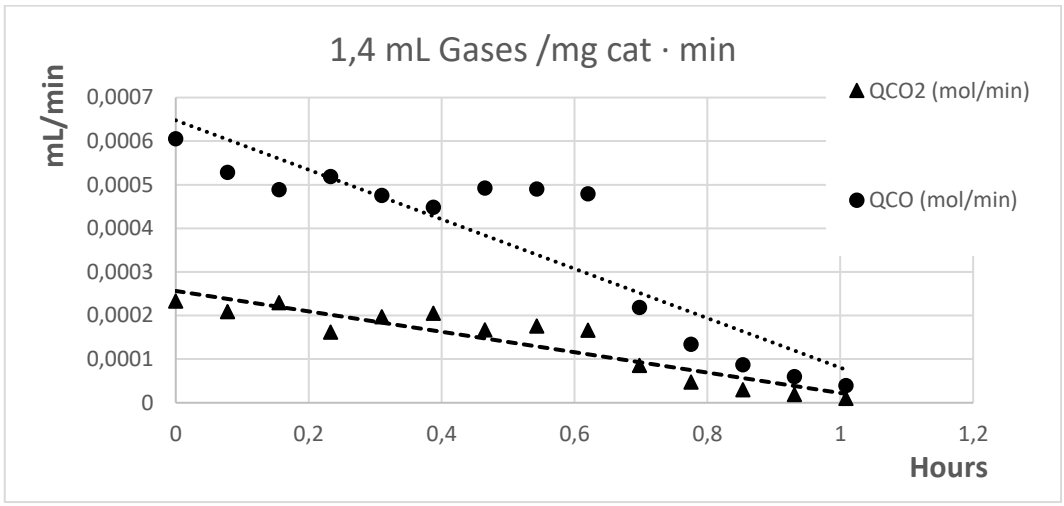

Fig.62. Selectivity of reaction products.

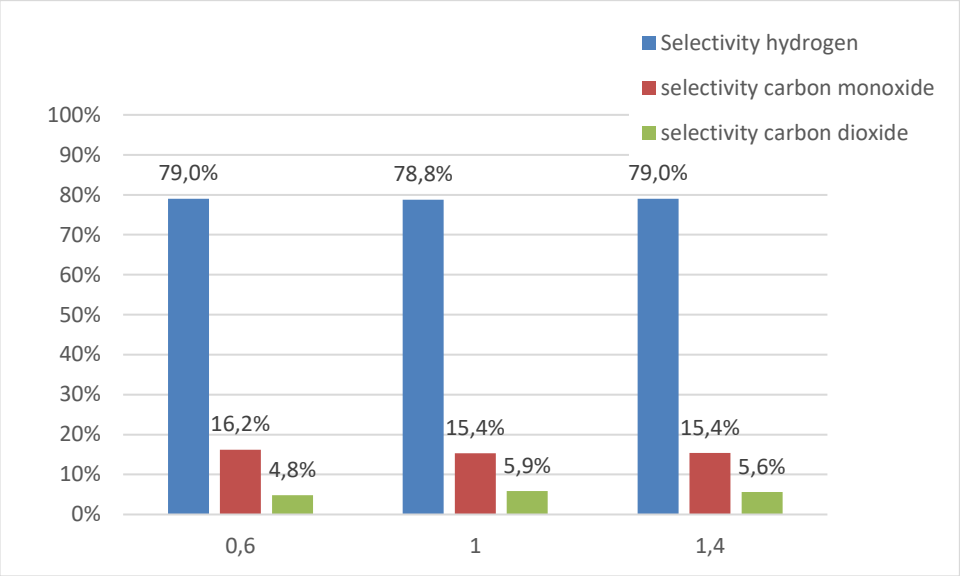

As concern the hydrogen production, increasing the flow of inlet gas, the hydrogen production increases until a maximum, and then, after the rapidly deactivation in the range of 1.4 $\frac{mL\ of\ inlet\ gas}{mg\ of\ catalys \cdot\ min}$, decreases quickly. This trend is observable in Fig.63.

Fig.63. Hydrogen production.

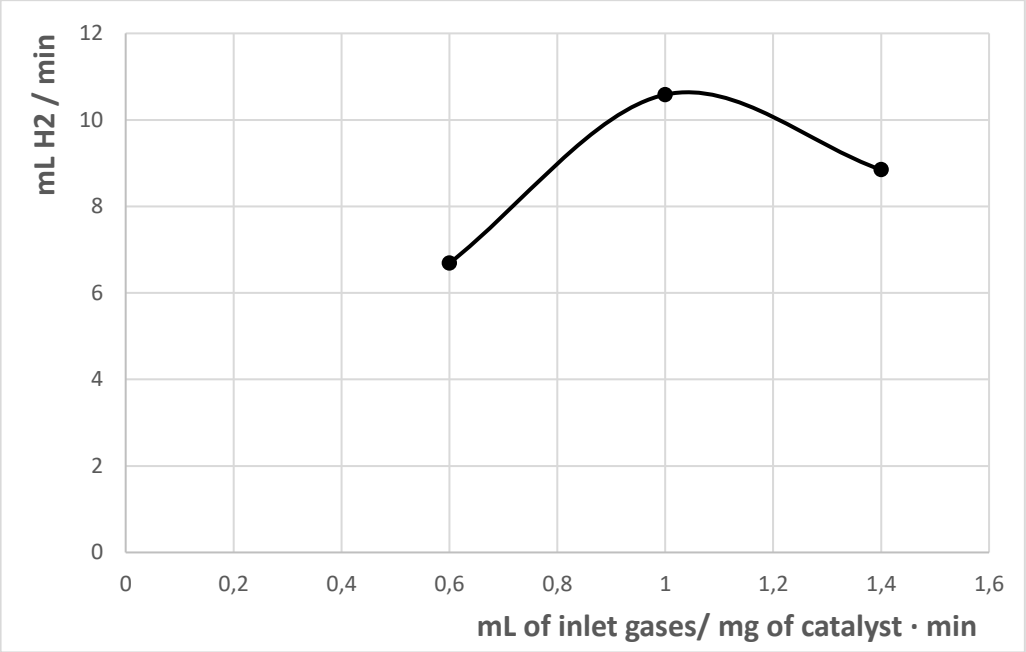

7.3 Regeneration of the catalyst.

In the previous chapter, the deactivation of the catalyst has been attributed to the deposition of carbon on the catalyst, but it cannot be sure if other deactivation processes are responsible of this. One of the processes of deactivation of the nickel catalyst during steam reforming is the sintering, because the reaction occurs at high temperature. Sintering is due to agglomeration of the crystallites of the active phase. It consequently opens the door to a decrease in activity [28]. According to the Rule of Tammann, sintering is generally to be expected at temperatures above 0.5 T_m, where Tm is the melting temperature of the metal in Kelvin [10]. It is thought that the type of alloy used with the thermal pre-treatment shall not undergo the sintering process. However, the main problem with sintering is the irreversibility of the process, and for this reason, it is important to investigate if the cause of deactivation is mainly due to the reversibility fouling or the irreversibility sintering.

Then, to understand which of the two processes prevails, one can try to regenerate the catalyst, and if this process resumes the catalytic activity, then the process is reversible and in particular attributable to fouling.

Carbonaceous deposits can be removed by gasification with O_2, H_2O, and H_2. However, gasification of more graphitic or less reactive carbons or coke species in H_2 or H_2O may require temperatures as high as 700–900 °C [28].

First of all, the steam reforming reaction was carried out in 2 rounds of 1 hour each, increasing the flow / weight ratio of the catalyst, as for the other tests.

However, the S / C ratio has been modified, starting from a lower ratio of 1.2 and increasing up to 1.75, in order to subject the catalyst to the fouling phenomenon more. Then, the regeneration test has been performed with steam at a temperature of 800 °C and a pressure of 1 bar. A the end a third round has been carried out to compare the rate of reactivation.

The catalyst has been deposited in the same manner of previous, but this time the weight of catalyst is 96 mg with an average of 5,3 $\frac{mg\ of\ catalys}{cm^2}$ each plate. The working conditions are summarized in Tab.12 .

Tab.12. Working condition for regeneration test.

$\frac{mL\ of\ inlet\ gases}{mg\ of\ catalys\ \cdot\ min}$	S/C	GHSV h^{-1}	$\frac{mL\ of\ inlet\ gases}{min}$
0,2	1,2	2813	19,2
0,6	1,4	8439	57,6
1	1,6	14065	96,0
1,4	1,75	19692	134,4

In the Fig.64 the methane conversion is shown for the first run for the different rates described in Tab.12 .

Fig.64 Methane conversion along the time, Run 1.

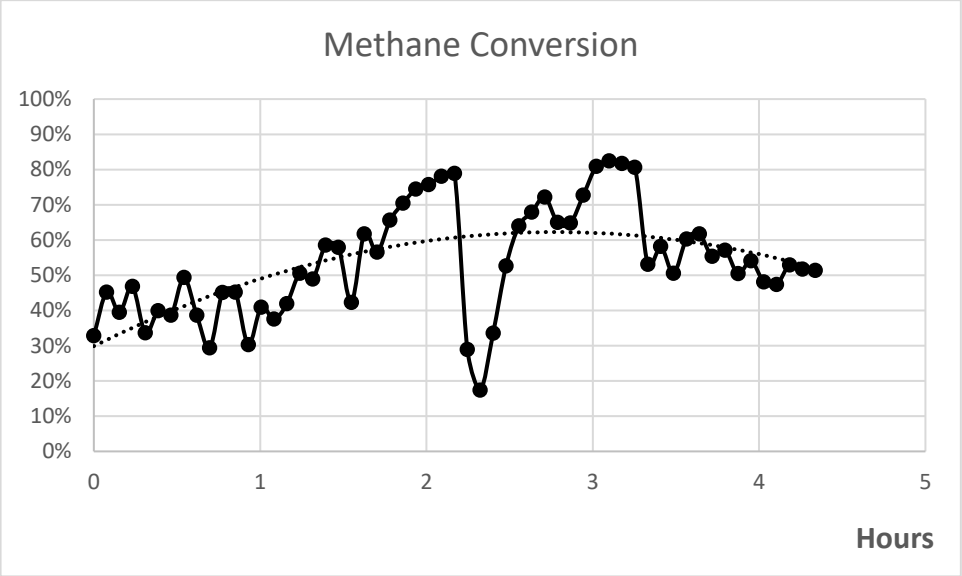

It shows that the conversion increases in the first part, because the steam carbon ratio is increasing, then, when the mass transfer is disadvantaged by excessive inlet flow, it returns to decrease. The methane conversion reaches here a higher maximum value than the first experiment in chapter 6 (around 80 %), because the amount of catalyst inside is greater.

In the Fig.65 is shown the methane conversion of the second run.

Fig.65. Methane conversion along the time, Run 2.

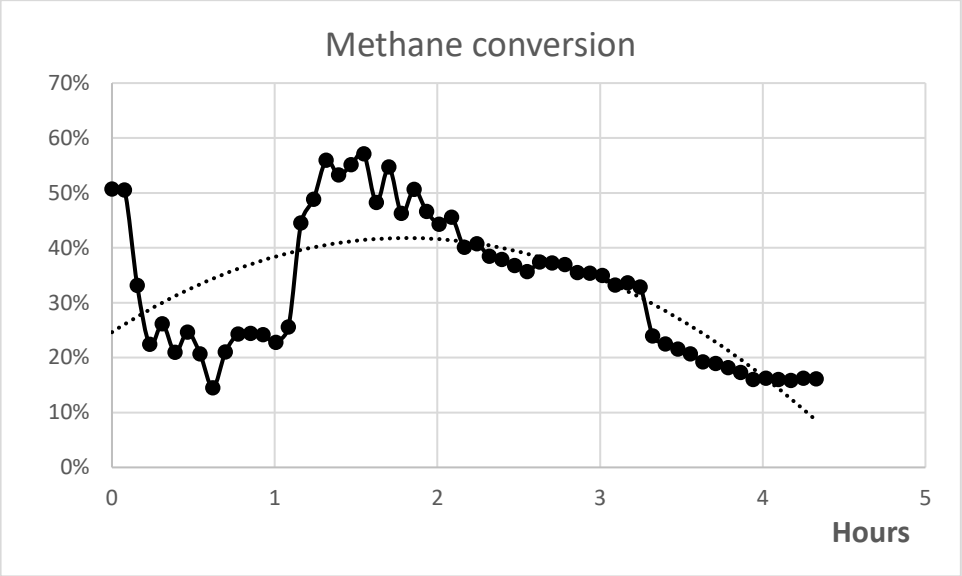

After the second round the catalyst has been regenerated with steam at 800 °C until the gas chromatograph no longer registers carbon dioxide and carbon monoxide. The methane conversion is reported on Fig.66.

Fig.66. Methane conversion, Run 3.

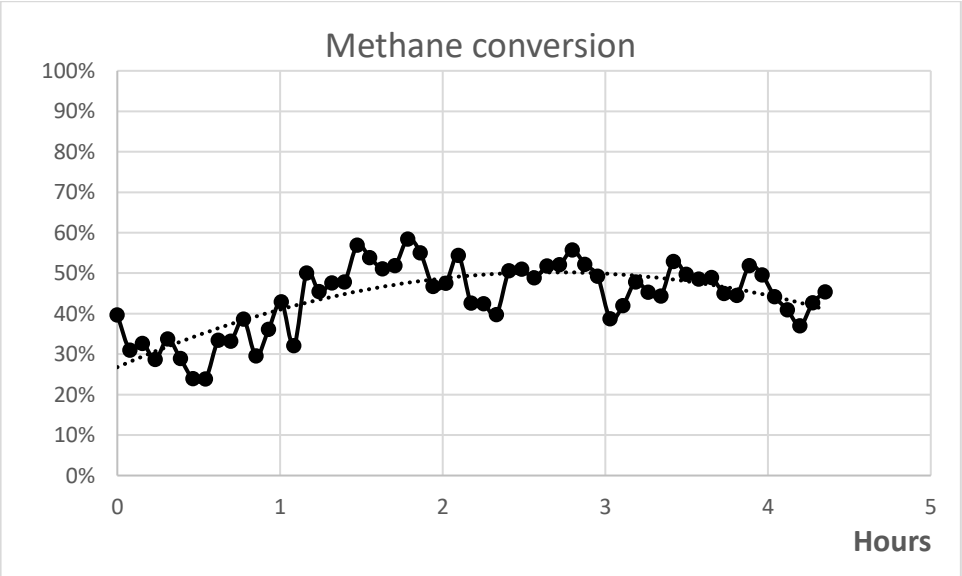

Fig.67 Methane conversion comparison.

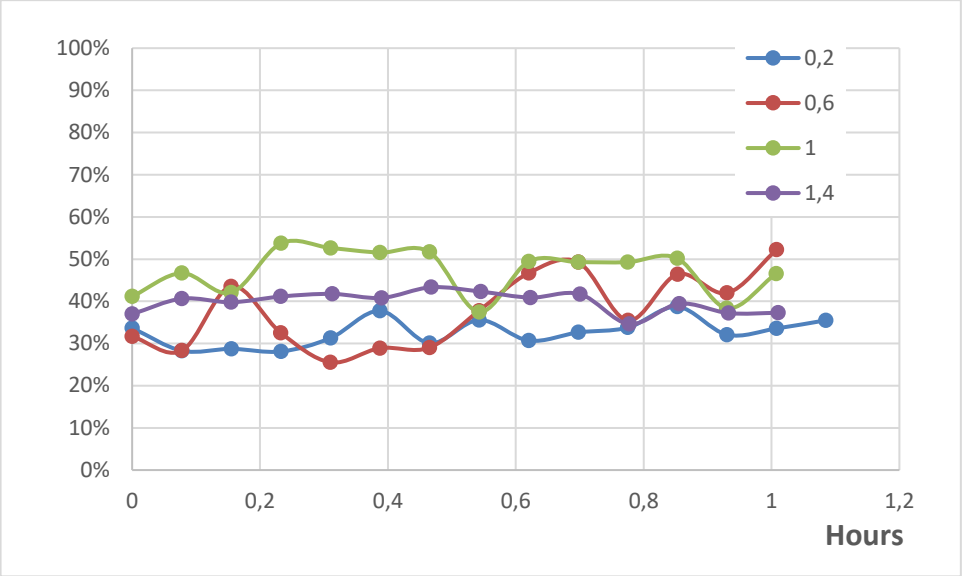

The conversion in the third run surpasses the one in the run 2, which means that the regeneration has been effective, although it does not reach the level achieved in the first one. This means that the catalyst partly undergoes the sintering and is partly loss in the flow. The gap of conversion irreversibly lost is observable on the Fig.68.

Fig.68. Methane conversion comparison between run 1, 2 and 3 for the different ratios flow / ratios.

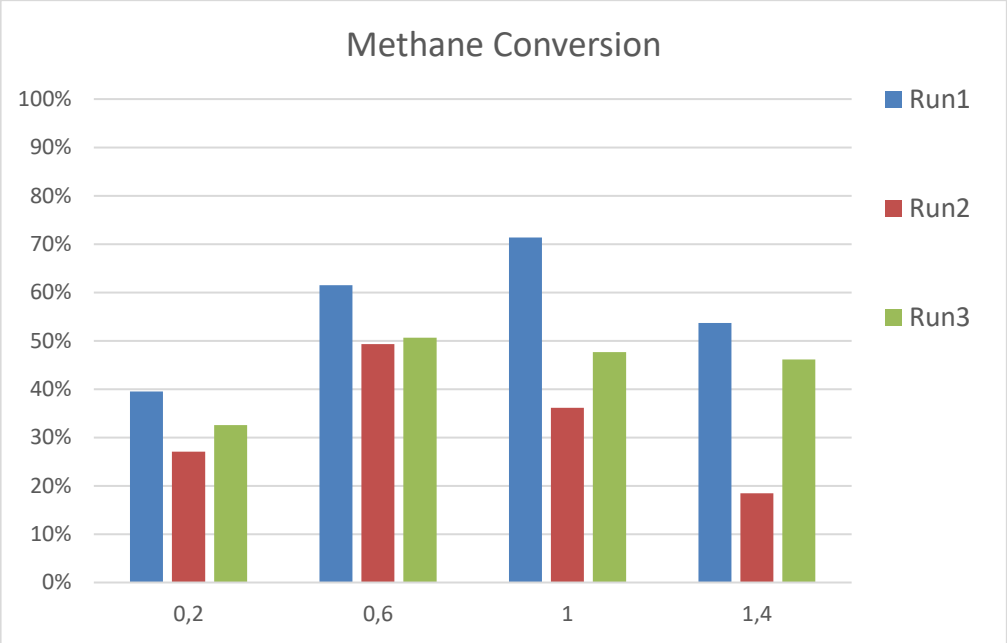

In the Fig.69 is shown the hydrogen production that follows the methane conversion trend. After the regeneration the catalyst recovers its activity, in particular in the areas of greatest stress, namely when the flow of inlet gases is high.

Fig.69. Hydrogen production for the different runs.

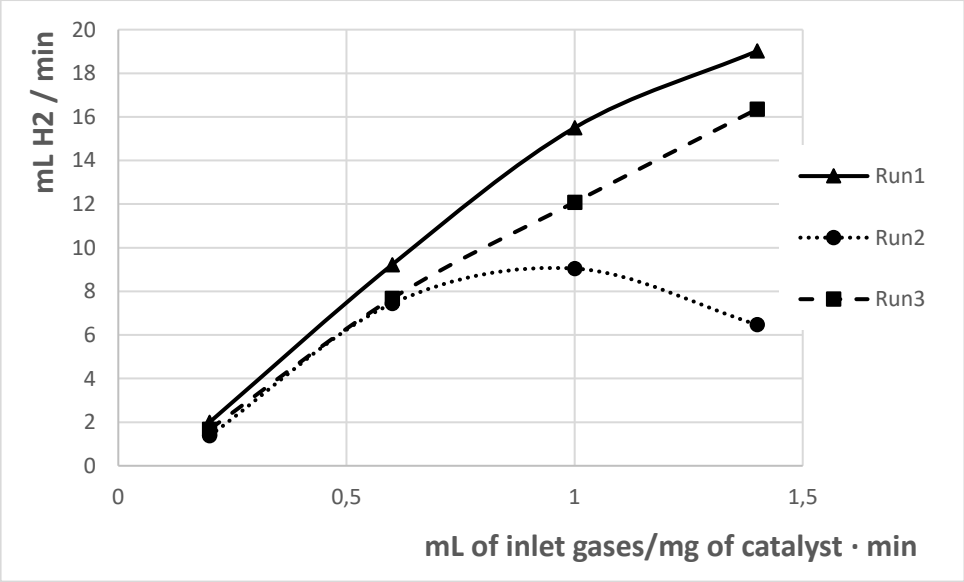

Indeed, the regeneration is possible with water steam obtaining good results, which has the advantage of being cheap compared to the other gases that could be used.

8. COMPARISON OF REACTORS PERFORMANCES

8.1. Reactors Performance.

To evaluate and analyse the performance of the micro-structured reactor, its performances must be compared with that of the cordierite monolithic reactor.

First of all, the tests have been carried out with a limitation on the minimum flow rate for the micro-structured reactor, and a limitation on the maximum for the cordierite one, so only the intermediate points of flow are comparable. A comparison of the methane steam reforming is shown in Fig.70.

Fig.70. Methane conversion for the two kind of reactor.

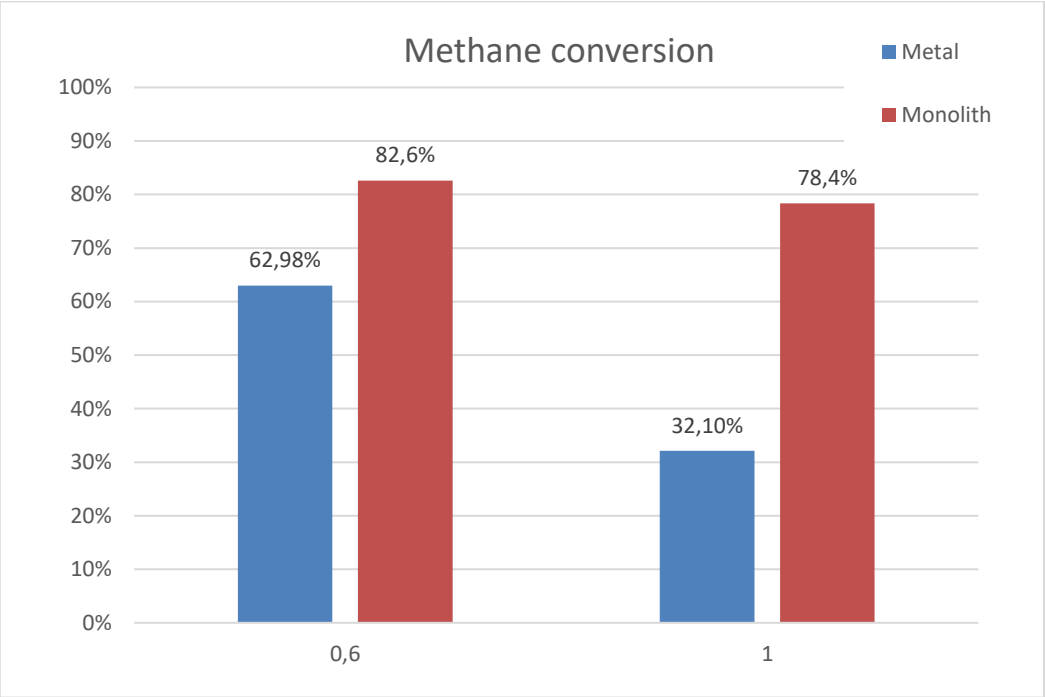

The micro-structured reactor has at most 20 % less conversion than the other, and this is due to the not perfect configuration of the channels of reactors, the inlet pore are not of the same size, and are numerically less.

Another problem is the higher pressure drop, which involves a greater fouling especially for higher gas flows.

Then it was compared the production of hydrogen but normalised with the amount of inlet gases. The results shown in Fig.71 reveals a gap around 20 %, when the inlet flow is 0,6 $\frac{mL\ of\ inlet\ gas}{mg\ of\ catalys \cdot min}$.

Fig.71. Production of hydrogen, comparison between micro-structured reactor and cordierite monolith.

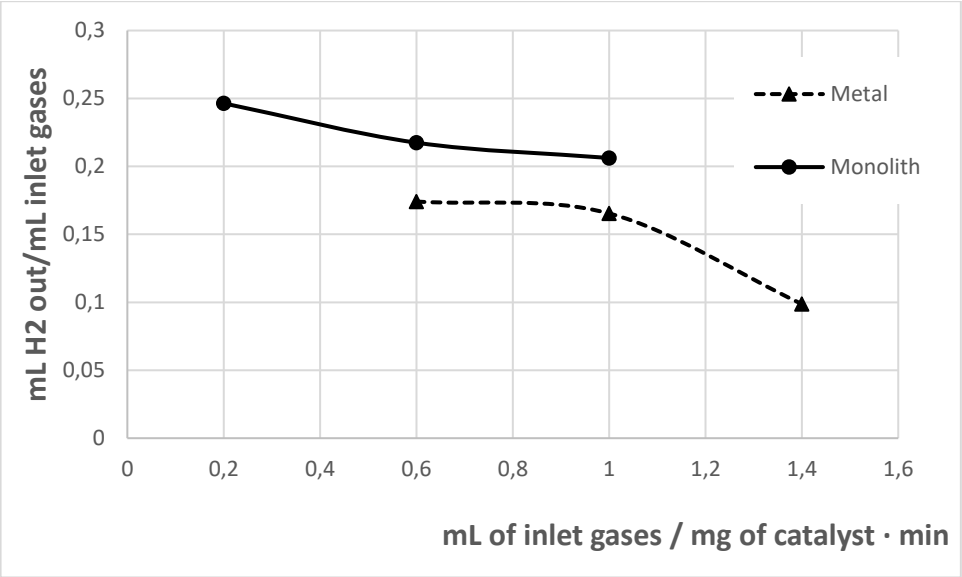

This result is possibly due to the not perfect mass and heat transfer management. In fact, once the test is complete and the reactor is dismantled, it is possible to notice that the plates collocated in the centre of the reactor are more stressed than the peripheral ones. It is shown on the red circle on the Fig.72.

Fig.72. Plates after the steam reforming test.

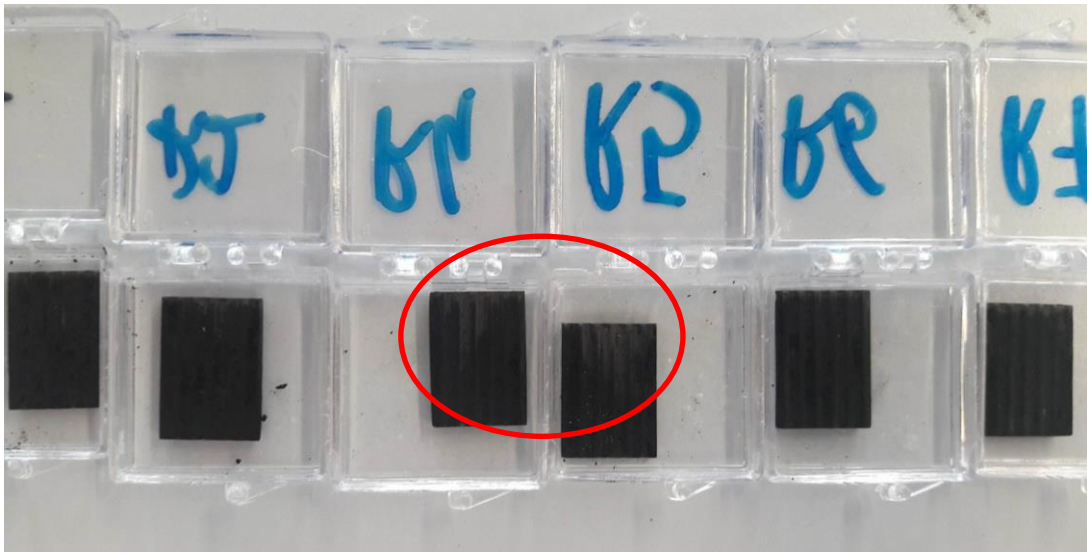

In Fig.73 the production of hydrogen of the run 1 before the catalyst regeneration (paragraph 7.3) hasbeen added to the Fig.71.

Fig.73 Production of hydrogen, comparison of the results between cordierite monolith (S/C=2), micro structured (S/C=2) and run 1 of micro-structured reactor (S/C in Table 12).

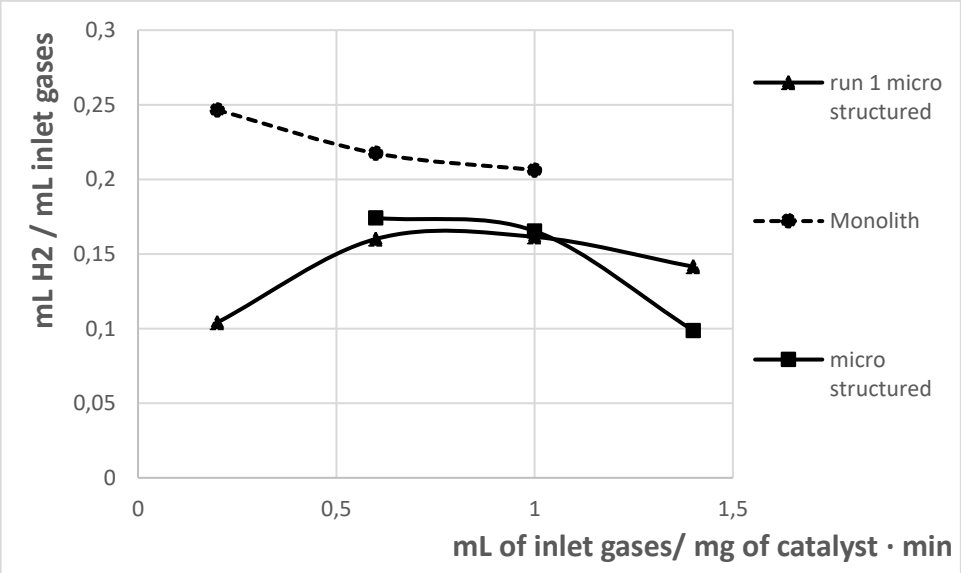

The results were expected: Taking into account that different S/C ratios were used (Tab.12), by increasing the S/C ratio from 1,2 to 1,75, the hydrogen production increases with the flow of inlet gases. Instead, keeping the steam to carbon ratio constant at a value of two, the hydrogen production decreases with the flow.

CONCLUSION

The main objective of this work was to verify if it is possible to deposit a catalyst on a FeCr alloy of a reactor for steam reforming, which is supplied by a company. The type of alloy used is not the most common, since it is usually preferred to build these kind of reactors with an alloy containing aluminium (FeCrAlloy) in order to form an aluminium oxide layer which is the same of the support of the nickel catalyst directly in the thermal pre-treatment phase.

However, the results were positive. The catalyst was successfully deposited thanks to the heat-treatment, which causes the formation of a chromium oxide coat, which is able to increase the adherence of the support.

It has also been found a way to increase the adhesion through the pre - formation of an alumina layer between the chromium oxide and the catalyst coat

In addition, the regeneration of the catalyst via water steam was also possible, sign that the sintering phenomena, that can poison the catalyst, did not prevail over the fouling ones.

Although it was expected, the results obtained are worse than those obtained with the cordierite reactor: the overall performance is around 20% less.

The use of the micro-structured reactor combined with a SOFC may still be advantageous from an energetic and economic point of view, since the reaction is strongly endothermic and the management of the heat is easier with a metal reactor. However, this aspect has not been investigated and further analysis is needed.

LIST OF FIGURES

LIST OF TABLES

Bibliography

[1] R.J. Braun, S.A. Klein, D.T. Reindl, *Evaluation of system configurations for solid oxide fuel cell-based micro-combined heat and power generators in residential applications*, J. Power Sources. 158 (2006) 1290–1305.

[2] I. EG&G Technical Services, *Fuel Cell Handbook*, Fuel Cell. 7 Edition (2004) 1–352.

[3] R. Napoli, M. Gandiglio, A. Lanzini, M. Santarelli, *Techno-economic analysis of PEMFC and SOFC micro-CHP fuel cell systems for the residential sector*, Energy Build. 103 (2015) 131–146.

[4] K.U. Birnbaum, J. Linssen, P. Leifeld, *Reduction of Residental Carbon Dioxide Emissions Through the Use of Small Cogeneration Fuel Cell Systems*, (2008) 11–21.

[5] J.A. Moulijn, M. Makkee, A.E. Van Diepen, Chemical process technology, 2013.

[6] J.G. Xu, G.F. Froment, *Methane Steam Reforming, Methanation and Water-Gas Shift .1. Intrinsic Kinetics*, Aiche J. 35 (1989) 88–96.

[7] J. R. Rostrup-Nielsen, Catalytic Steam Reforming, 1984.

[8] J.R. Rostrup-Nielsen, J. Sehested, J.K.B.T.-A. in C. Nørskov, *Hydrogen and synthesis gas by steam- and C0₂ reforming*, 47 (2002) 65–139.

[9] H. Wu, V. La Parola, G. Pantaleo, F. Puleo, A. Venezia, L. Liotta, *Ni-Based Catalysts for Low Temperature Methane Steam Reforming: Recent Results on Ni-Au and Comparison with Other Bi-Metallic Systems*, Catalysts. 3 (2013) 563–583.

[10] P. va. Beurden, *On The Catalytic Aspects Of Steam Reforming Methane - A Literature Survey*, Ecn. (2004) 1–27.

[11] F. Frusteri, S. Freni, L. Spadaro, V. Chiodo, G. Bonura, S. Donato, S. Cavallaro, *H₂ production for MC fuel cell by steam reforming of ethanol over MgO supported Pd, Rh, Ni and Co catalysts*, Catal. Commun. 5 (2004) 611–615.

[12] Z. Zhang, X.E. Verykios, *Carbon dioxide reforming of methane to synthesis gas over Ni/La2O3 catalysts*, Appl. Catal. A Gen. 138 (1996) 109–133.

[13] M.C. Annesini, V. Piemonte, L. Turchetti, *Carbon Formation in the Steam Reforming Process: a Thermodynamic Analysis Based on the Elemental Composition*, Chem. Eng. Trans. 11 (2007) 21–26.

[14] S. Helveg, J. Sehested, J.R. Rostrup-Nielsen, *Whisker carbon in perspective*, Catal. Today. 178 (2011) 42–46.

[15] B. Béguin, E. Garbowski, M. Primet, *Stabilization of alumina by addition of lanthanum*, Appl. Catal. 75 (1991) 119–132.

[16] R. Martínez, E. Romero, C. Guimon, R. Bilbao, *CO_2 reforming of methane over coprecipitated Ni-Al catalysts modified with lanthanum*, Appl. Catal. A Gen. 274 (2004) 139–149.

[17] M. Ozawa, K. ichi Araki, *Effect of La modification on the stability of coating alumina layer on FeCrAl alloy substrate*, Surf. Coatings Technol. 271 (2015) 80–86.

[18] T.B. Stachowiak, T. Rohr, E.F. Hilder, D.S. Peterson, M. Yi, F. Svec, J.M.J. Fréchet, *Fabrication of porus polymer monoliths covalently attached to the walls of channels in plastic microdevices*, Electrophoresis. 24 (2003) 3689–3693.

[19] R.M. Heck, S. Gulati, R.J. Farrauto, *The application of monoliths for gas phase catalytic reactions*, Chem. Eng. J. 82 (2001) 149–156.

[20] J.L. Williams, *Monolith structures, materials, properties and uses*, Catal. Today. 69 (2001) 3–9.

[21] T.A. Nijhuis, A.E.W. Beers, T. Vergunst, I. Hoek, F. Kapteijn, J. Moulijn, *Preparation of monolithic catalysts*, Catal. Rev. 43 (2001) 345–380.

[22] C. Agrafiotis, A. Tsetsekou, *Deposition of meso-porous γ-alumina coatings on ceramic honeycombs by sol-gel methods*, J. Eur. Ceram. Soc. 22 (2002) 423–434.

[23] G. Di Caprio, *Gli Acciai Inossidabili*, (n.d.).

[24] O.H. Laguna, M.I. Domínguez, M.A. Centeno, J.A. Odriozola, Catalysts on Metallic Surfaces: Monoliths and Microreactors, Elsevier B.V., 2016.

[25] Y. Diaz, A. Sevilla, A. Mónaco, F.J. Méndez, P. Rosales, L. Garcí, J.L. Brito, *Metallic monoliths of AISI 304 stainless steel, aluminum, FeCrAlloy® and brass, coated by Mo and W oxides for thiophene hydrodesulfurization*, Fuel. 110 (2013) 235–248.

[26] V. Meille, *Review on methods to deposit catalysts on structured surfaces*, Appl. Catal. A Gen. 315 (2006) 1–17.

[27] L. Zhang, Y. Ren, Q. Luo, X. Ying, H. Xu, J. Xuan, *A Novel Method to from Well-adhered γ-Al2O3 Coating in 316L Stainless Steel Microchannels*, Energy Procedia. 75 (2015) 2044–2048.

[28] M. Argyle, C. Bartholomew, *Heterogeneous Catalyst Deactivation and Regeneration: A Review*, Catalysts. 5 (2015) 145–269.